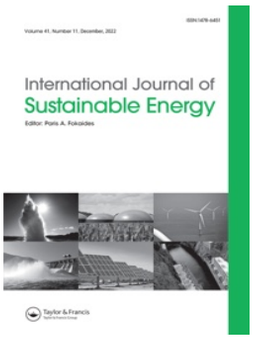

International Journal of Sustainable Energy

ISSN: 1478-6451 (Print) 1478-646X (Online) Journal homepage: www.tandfonline.com/journals/gsol20

Thermodynamic analysis of a novel high-temperature heat pump cycle with inter cooled compression and reheated expansion based on the reversed Brayton cycle

Nancy Kabat, Enrico Jende, Fatma Cansu Yücel & Panagiotis Stathopoulos

To cite this article: Nancy Kabat, Enrico Jende, Fatma Cansu Yücel & Panagiotis Stathopoulos (2025) Thermodynamic analysis of a novel high-temperature heat pump cycle with inter cooled compression and reheated expansion based on the reversed Brayton cycle, International Journal of Sustainable Energy, 44:1, 2515452, DOI: 10.1080/14786451.2025.2515452

To link to this article: https://doi.org/10.1080/14786451.2025.2515452

Published online: 26 Jun 2025.

INTERNATIONAL JOURNAL OF SUSTAINABLE ENERGY
2025, VOL. 44, NO. 1, 2515452
https://doi.org/10.1080/14786451.2025.2515452

Thermodynamic analysis of a novel high-temperature heat pump cycle with inter cooled compression and reheated expansion based on the reversed Brayton cycle

Nancy Kabat, Enrico Jende, Fatma Cansu Yücel and Panagiotis Stathopoulos

German Aerospace Center (DLR), Institute of Low-Carbon Industrial Processes Cottbus, Germany

ABSTRACT

High-temperature heat pumps offer a promising approach to deliver CO_2-neutral process heat by upgrading waste heat with electricity from renewable resources. In this work, a heat pump cycle including inter cooled compression and reheated expansion is presented and compared to the simple Brayton cycle. Numerical simulations are used to investigate the provision of process heat at 250°C and process cooling at −30°C. An exergy analysis and parameter study is carried out. The results show an improved performance of the complex cycle as a result of more efficient temperature profiles improving the exergy utilisation. While previous studies often consider idealised process variants or are focused on individual purposes, the present work contributes to the analysis and evaluation of complex cycles with multi-stage process control while simultaneously supplying heat and cold. A deeper understanding of the thermodynamic interactions provides a reliable basis for the energy-related design of systems with multiple temperature levels.

ARTICLE HISTORY
Received 16 September 2024
Accepted 7 May 2025

KEYWORDS
High-temperature heat pump; Brayton cycle; inter cooled compression; reheated expansion; exergy analysis; parametric study

Nomenclature

C	compressor
COP	coefficient of performance
c_p	specific heating capacity [kJ/kgK]
c	cold
ch	chemical
DLR	German Aerospace Center
EU	European Union
$\dot{E}x$, ex	exergy flow, specific exergy [kW, kJ/kg]
ϵ	effectiveness [–]
η	isentropic efficiency [–]
η_{ex}	exergetic efficiency [–]
GA	genetic algorithm
GHG	greenhouse gas
$\dot{H}$, h	enthalpy flow, specific enthalpy [kW, kJ/kg]
h	hot

CONTACT Nancy Kabat Nancy.Kabat@dlr.de

HTHP	high temperature heat pump
HTHX	high temperature heat exchanger
HX	heat exchanger
IEA	International Energy Agency
IHX	internal heat exchanger
k	kinetic
LMTD	logarithmic mean temperature difference
LTHX	low temperature heat exchanger
$\dot{m}$	mass flow [kg/s]
mech	mechanical
NZE	net zero emissions
P	power [kW]
p	pressure [bar]
p	potential
ph	physical
Π	pressure ratio [-]
Ψ	exergy efficiency [-]
$\dot{Q}$	heat flow [kW]
R	controller
$\dot{S}$, s	entropy flow, specific entropy [kW/K, kJ/kgK]
T	turbine
T	temperature [°C, K]
TM	turbo machine
th	thermal
tot	total
ΔT_{Lift}	temperature lift [K]
ΔT_m	logarithmic mean temperature difference [K]

1. Introduction

According to the International Energy Agency (IEA) the worldwide CO_2 emissions have risen to a new high of 36.8 Gt in 2022. Even though industry-related emissions fell by 1.7% to 9.2 Gt compared to 2021, the industry sector continues to be a large greenhouse gas (GHG) emitter. The global energy consumption of the industry sector in 2022 amounts to 37% or 166 EJ of the total consumption. To further accelerate the reduction of industry-related emissions and achieve net zero emissions (NZE) by 2050, more low-carbon technologies, such as direct electrification and high-temperature heat pumps (HTHP), must be integrated into industrial processes (IEA 2023, 2024). Currently, the industrial demand for fossil fuels accounts for about one-fifth of the total natural gas consumption. The use of HTHPs can lead to a rapid decline in the demand for fossil fuels for industrial process heating and plays a key role in the decarbonisation of industrial sectors. Heat pumps are able to generate temperatures of up to 160°C by processing waste heat, making them ideal for the application in the paper, food and chemical industry. Therefore, HTHPs could cover a wide range of heat requirements for industrial processes below 200°C, which accounts for around 30% of the total industrial heat demand (IEA 2022). Due to their great potential, heat pumps are already used to provide process heat below 100°C. However, there are currently only a few operational models for the use at temperatures up to 200°C (Heat Pumping Technologies 2022). This makes it all the more important to continue research in this area. This research of heat pump cycles for the simultaneous provision of process heat up to 200°C and process cooling below 0°C extends already existing work on the use of heat pumps in industry with regard to higher application ranges for process temperatures. The introduction of this article

discusses the scientific literature on heat pumps. The use of heat pumps in various industries and the relevance of the heat pump cycle configuration is presented.

A literature review of supercritical CO_2 (sCO_2) Brayton cycles and the influence of operating parameters on the heat pump performance is given. Furthermore, studies on the use of heat pumps in industry for process heating and simultaneous cooling are examined. Finally, a review of the literature on the application of exergy analysis shows the relevance of this method for the thermodynamic evaluation of heat pump systems. Subsequent to the literature research, the Brayton heat pump cycles to be examined and the heat pump thermodynamics are presented.

1.1. Literature review

Several studies investigated the role of HTHPs in the scope of decarbonisation strategies in industrial sectors. Dumont et al. (2023) investigated the techno-economic feasibility of new HTHP technologies integrated into processes in the food and beverages industry in Germany. The results have shown that 12TWh of process heat demand in this sector could be covered by the use of HTHP technologies. Schlosser et al. (2020) analysed 155 case studies on large – scale heat pumps. They identified suitable industry-related processes such as drying and thermal preservation that can be supplied with commercially available heat pump technologies. Kosmadakis (2019) investigated the potential of industrial heat pumps in the EU industry. The results of this analysis show that the total heat supply potential in the temperature range between 100°C and 200°C of industrial heat pumps in the EU is 28.37 TWh/year. The food, paper, non-metallic minerals, and non-ferrous metals industry sector were identified as the most promising ones for the application of heat pumps. Zühlsdorf et al. (2019) analysed heat pump concepts for the supply of process heat at high temperatures in industrial applications. The results showed that it is possible to provide process heat economically with electrically powered heat pumps at temperatures of up to 280°C. The reversed Brayton cycle was suggested as a solution for applications with large temperature glides. Rehfeldt, Fleiter, and Toro (2018) estimated the heating and cooling demand in the EU industry and analysed the different industrial sectors and the associated temperature levels of the processes. In the paper, food, and chemical industry, a large demand for process heat in the range of 100°C to 500°C for drying and separation processes was identified. In particular, the food, beverage, and tobacco industry were found to have a demand for process cooling in the temperature range of −30°C to 15°C. Bataille et al. (2018) mentioned heat pumps as a possible option for process heat supply up to 250°C and emphasised the importance of CO_2 emission-free technologies for the industry. An overview of the state of the art HTHPs was provided in the Annex 58, Task 1 (Heat Pumping Technologies 2022). This report lists available heat pump technologies with capacities between 30 and 70 kW and maximum temperatures between 100°C and 280°C. Arpagaus et al. (2018) investigated the state of the art of HTHPs with heat sink temperatures in the range of 90°C to 160°C. Most heat pump cycles used single-stage configurations with heating capacities from 20 kW to 20 MW. An internal heat exchanger was mentioned to achieve cycle optimisation. The coefficient of performance (COP) ranged from 2.4 to 5.8 at temperature lifts between 95 and 40 K. The authors also mentioned the food, paper, metal and chemical industry sector as the greatest potential for heat pump

technology application. The literature research proves the wide range of applications for HTHPs in the industry, mainly for providing process heat but also process cooling.

Although the use of HTHPs to provide process heat for industry can be applied in various industrial sectors, it requires precise adaptation of the heat pump to the given process conditions. There are some studies that deal with the configuration of the heat pump cycle and its advantages and disadvantages for certain applications. Gai et al. (2020) investigated the performance and integration of different types of heat pumps in different processes. The results showed that the optimal application range depends on different heat pump types. The authors also mentioned the importance of a heat pump's ability to provide heating and cooling at the same time, especially in industry. Adamson et al. (2022) reviewed 49 existing high-temperature or trans-critical heat pump cycle configurations with different temperature ranges. As a result, a classification of ten performance-enhancing cycle components was carried out. Wolf (2022) investigated and compared various sCO_2 power cycle configurations with standardised boundary conditions in terms of thermal efficiency. Ambient air was selected for the condensation of CO_2 at the heat sink. The heat source temperatures were varied between 60°C and 100°C. It was shown that adding additional components to the basic cycle configuration lead to a change in efficiency. The results showed that an additional heat exchanger for heat source recuperation and extraction has a positive effect on the efficiency of the cycle, while at low temperatures the inter cooled compression reduces the performance. Marchionni, Bianchi, and Tassou (2018) investigated eight sCO_2 Joule-Brayton cycles. A parametric study showed that the turbine inlet temperature had the greatest influence on the cycle performance. It was also shown, that the most complex configuration lead to a higher overall efficiency. Angelino and Invernizzi (1995) considered the reversed Brayton cycle to be a suitable option for supplying heat at high temperatures. In the literature, the reversed Brayton cycle is often mentioned as a suitable cycle for heat pump technologies. It is also mentioned, that the configuration of the heat pump cycle itself is an important aspect in order to fulfil the specific process requirements.

A frequently used configuration of the Brayton cycle is the utilisation of supercritical CO_2 as the working fluid. The sCO_2 Brayton cycle is often used to examine heat pump performance influences due to its high potential to achieve significantly high efficiency. Ahmed and Ehsan (2023) investigated the design and off-design of a printed circuit heat exchanger as a precooler in an indirect cooling system for a sCO_2 re-compression cycle. The performance of the off-design at different inlet temperatures and pressures was analysed to optimise heat transfer rates. The study showed a superior influence of water-cooled systems for the inlet temperature of the sCO_2 compressor compared to air-cooled systems. Several studies of Ehsan et al. are addressing dry cooling systems in sCO_2 power cycles for concentrated solar energy applications. The authors (Ehsan et al. 2023) examined the current state of sCO_2 cycles as well as the progress made in components such as turbo machinery and heat exchangers for these systems. Various layouts of sCO_2 power cycles that can be used in different energy sectors are presented. The study outlines the need for improvement of the performance of recuperator and turbo machinery. Ehsan et al. (2020b) furthermore addressed the feasibility of dry cooling systems in sCO_2 power cycles for concentrated solar power applications. The authors explored the potential advantages over conventional Rankine cycles. The

importance of the cooling system design for the performance of the cycle is emphasised. In another study, the authors (Ehsan et al. 2020a) presented a comprehensive thermal evaluation of dry cooling systems in sCO_2 power cycles for concentrated solar power applications. A novel approach to optimising the main compressor inlet temperature was presented. The results underscore the importance of optimising compressor inlet temperatures and inter-stage pressure to improve thermal performance. In an additional study, Ehsan et al. (2020c) evaluated the performance of a dry-cooled CO_2 plant under various ambient and solar radiation conditions. Again, the importance of the design point compressor inlet temperature on the system performance is emphasised. Furthermore, the importance of an additional bypass arrangement to maintain design point conditions at low ambient temperatures is highlighted. A further work of the authors (Ehsan et al. 2019a) deals with the investigation of the performance of a dry-cooled sCO_2 re-compression cycle. Seven performance indicators were defined to evaluate the seasonal performance of a natural draft dry cooling tower plant. The results show that the thermal performance is significantly affected by ambient temperature variations, which in turn affects the efficiency of the cycle. Ehsan et al. (2019b) also investigated the effects of cooling system design on the thermal performance of a sCO_2 re-compression cycle and did an economic analysis, considering various cost and performance indicators as well as the effects of sCO_2 inlet temperatures and ambient air fluctuations. Another study (Ehsan, Guan, and Klimenko 2018a) deals with the investigation of heat transfer properties and correlations of sCO_2 under heating and cooling conditions in horizontal tubes. The study highlights the influence of various operating parameters on the heat transfer and pressure drop of sCO_2. Ehsan et al. (2018c) also investigated the design of natural draft dry cooling towers for a 25 MW solar power plant using the sCO_2 Brayton cycle. A performance analysis of air-cooled heat exchangers under various operating conditions was carried out. The results show that the sCO_2 inlet temperature and operating pressure strongly influence the cooling system performance. The study highlights the importance of optimising the effectiveness of the recuperator for an accurate cycle performance analysis. Ehsan et al. (2018b) further developed a validated MATLAB code for a dry cooling unit for a 25 MW solar power plant with a sCO_2 Brayton cycle. Both direct and indirect cooling systems are designed and compared under different ambient temperatures and operating conditions. The results show that dry cooling systems perform better at high ambient temperatures than indirect systems and lead to lower sCO_2 outlet temperatures. The number of studies examining sCO_2 Brayton cycles indicates the importance of applying the Brayton cycle in terms of efficient waste heat utilisation. Often, the focus of the studies is on the development of efficient heat exchangers, turbines and compressors, as these significantly influence the efficiency of the entire cycle. The application of the sCO_2 Brayton cycle in cooling towers further highlights the significance of this cycle for cooling applications.

Since the performance and the temperatures that can be reached by a heat pump are crucial for its use in process applications, some studies are focusing on the investigation of heat pump performance and the achieved temperature lift. Mateu-Royo et al. (2018) investigated five vapour compression system configurations. They analysed the energy performance using different working fluids for heat delivery at temperatures of 110°C, 130°C and 150°C with various temperature lifts. They showed that a single-stage cycle with an internal heat exchanger is the most efficient configuration at lower temperatures.

At higher temperatures, the two-stage cycle with an internal heat exchanger showed the highest efficiency. Wu et al. (2023) carried out an energetic and exergetic investigation on a cascade heat pump, a recuperative heat pump and a carbon dioxide heat pump with different temperature lifts. They found the recuperative heat pump to be most suitable for direct-heating. A COP of 4.81 with a temperature lift of 60°C was reported. Gao, Xu, and Wang (2021) carried out investigations on a novel air-source hybrid absorption-compression heat pump. They compared the system with a conventional air-source heat pump and achieved a temperature lift over 90 K. With an increasing temperature lift from 70°C to 110°C, the COP decreased from 1.7 to 1.2. Sun, Guo, and Gong (2019) investigated three single-stage compression air-source heat pumps with a heat supply temperature of 90°C and a temperature lift of 68 K. They pointed out that the temperature glide of the refrigerant plays a crucial role in reducing irreversible losses during condensation and heat recovery. Jende et al. (2023) did a thermodynamic analysis of an integration of a reversed Brayton high-temperature heat pump into a food process. The authors present various integration strategies for integrating a reversed Brayton heat pump in a food production process and providing heat sink temperatures of 250°C at high-temperature lifts. A process integration into a thermal oil cycle and a direct integration at the process heat exchanger is investigated. The results show that a direct integration is more effective, but requires a good redesign to fit into the process. Most studies examine heat pumps with small temperature lifts, and a few studies are already looking at high-temperature lifts of over 90 K. However, the studies on high-temperature lifts with heat sink temperatures above 150°C are expandable.

As mentioned before, the simultaneous generation of process heat and cold by using heat pumps can be a new approach to the efficient use of waste heat, especially in the food industry. Nevertheless, the existing literature dealing with the simultaneous provision of process heat and process cooling for industrial applications is less common. Byrne and Ghoubali (2019) did an exergy analysis for two prototype air-source heat pumps for simultaneous heating and cooling. Three different operating modes to provide heating and cooling energy for buildings have been developed: a heating mode, a cooling mode and a simultaneous mode. The highest exergy destruction was found in the compressors. The results showed a direct influence of the component and system design on the exergy destruction. The authors emphasised the importance of conducting an early exergy analysis in order to identify and minimise component-related exergy destruction. Arunwattana (2022) proposed a design of a heat pump for simultaneous space heating and cooling. The COP evaluated for the cooling mode ranged around 5.0 and for the simultaneous mode around 6.3. The results show that the heat pump system under investigation can replace both the conventional air conditioning system and the electric water heater for residential buildings. Ayou, Hargiyanto, and Coronas (2022) investigated two ammonia-based compression heat pumps for simultaneous heating and cooling in a milk pasteurisation process with a cold water inlet temperature of 2°C and a heat output temperature in the range of 65–95°C. The performance of the systems was investigated and a parametric study was carried out. The results showed that such heat pump systems are more efficient solutions than the heating and cooling systems currently in use, as they can save up to 59% of primary energy. The development of such types of multi-stage compression heat pumps with a large temperature lift contributes significantly to decarbonisation in the industry. Ahrens et al. (2021) investigated

an integrated heat pump system of a green-field dairy. The authors determined the energy consumption and system performance by carrying out an energy analysis. The results showed that the integrated system, consisting of three different heat pump systems, is able to fulfil the temperature levels from 20°C to 95°C for the different consumers. The small number of studies that have been conducted on heat pumps for simultaneous provision of process heat and cooling mainly relate to applications in residential or office buildings and few examples being used in the food industry relate to their application in dairies with process temperatures below 100°C. There are currently hardly any simulative or experimental studies of industrial heat pumps for the simultaneous provision of process heat and cold at higher process temperatures. The contribution of such work would significantly increase the range of applications and the acceptance of end users in the industry.

A frequently used method for analysing a heat pump system is an exergy analysis, also known as a second law analysis. The exergy analysis is a suitable method for evaluating systems in terms of their efficiency and for localising exergy losses and exergy destruction due to irreversibilities. The results can indicate possibilities for component optimisation and thus increase the economic efficiency of the heat pump system. Kotas (1985) has described the methodology and advantages of an exergy analysis in detail. Several studies evaluated heat pump systems by using the exergy analysis method. Sarkar (2009) examined a sCO_2 Brayton cycle with re-compression. Using exergy analysis, he examined the effects of various operating parameters on the energy and exergy efficiency and the irreversibilities of the components. The results showed that the change in operating parameters has a greater influence on the irreversibility of the recuperator than on the turbo components.

Padilla et al. (2015) carried out exergy analyses on various sCO_2 Brayton cycles. The authors examined a simple Brayton cycle, a Brayton cycle with re-compression, a partial cooling cycle with re-compression and a re-compression cycle with intercooling of the main compression. All cycles were analysed using exergy analysis. Of all the cycles examined, the simple Brayton cycle had the lowest thermal and exergetic efficiency, but the authors emphasised the advantages of the simplicity and compactness of this cycle. Byrne and Ghoubali (2019) examined two heat pump prototypes with R407C and R290 as working fluids for simultaneous heating and cooling using an exergy analysis. In both prototypes, the compressor and the heat exchangers were the main sources of exergy losses in the system. Mateu-Royo et al. (2019) conducted an energy and exergy analysis of a HTHP prototype for waste heat recovery at heat sink temperatures between 90°C and 140°C and heat source temperatures between 60°C and 80°C. The COP varied between 2.23 and 3.41 and the heating capacity between 10.9 and 17.5 kW. The authors mentioned the compressor to have the highest potential improvement to reduce exergy destruction in the system and confirmed the benefit of an internal heat exchanger on the system performance. The experimental results show that the effectiveness of the internal heat exchanger increases with an increasing heat sink temperature. Especially in high-temperature applications, an internal heat exchanger therefore has a major influence on system performance. The authors also showed the influence of the heat sink temperature on the COP and the strong dependence of the heating capacity on the heat source temperature. Dai et al. (2020) proposed five configurations of dual-pressure condensation HTHPs. They carried out a thermodynamic analysis and

compared the performance of the systems to single-stage, two-stage and cascade systems. The results showed that the use of dual-pressure condensation HTHPs can reduce the exergy destruction in the system due to an improved thermal matching in the condensers. This significantly reduces the irreversible losses due to heat transfer between the refrigerant and the heat transfer medium, thereby improving the energy efficiency of the system. The compressor was found to cause the highest exergy losses. Kabat, Oehler, and Stathopoulos (2025) submitted a paper for an exergy analysis based on experimental results of a heat pump demonstrator called 'CoBra' based on the reversed Brayton cycle. The heat pump prototype is built at the Institute of Low-Carbon Industrial Processes at the German Aerospace Center (DLR) and achieves heat sink temperatures over 200°C with air as the working medium. The literature review shows that exergy analysis is a common application for analysing heat pump systems in order to identify the exergy distribution in the system and to show possible improvement potentials.

In a previous work, Kabat et al. (2023) investigated nine different Brayton cycle heat pump configurations for simultaneous heating and cooling. All cycle configurations were analysed in terms of the COP using air as the working medium for the primary and secondary cycles at the heat sink and the heat source. The same boundary conditions were selected for all configurations to simultaneously ensure a heat sink temperature of 250°C and an outlet temperature at the heat source of −30°C to 5°C. The results of the simulation showed that the most efficient configuration was the most complex one, with five heat exchangers and four turbo machines for simultaneous provision of process cooling between −30°C and −15°C and process heating at 250°C, with a total COP of about 2.1. For the provision of process cooling in the temperature range between −10°C and 5°C, the standard recuperated Brayton cycle had the best performance with a total COP of 2.27. The results showed that the heat pump cycle configuration should be selected according to the temperature requirements for the simultaneous provision of process heat and cooling in order to obtain the best possible COP. The resulting complex cycle configuration with five heat exchangers and four turbo machines is selected as the heat pump cycle to be investigated for the present work in order to consider this heat pump cycle from an energetic and exergetic point of view.

The large number of studies on HTHPs shows the relevance of heat pump technology for industrial application. The reversed Brayton cycle is recommended as a simple and efficient application for an industrial heat pump cycle to provide process heat and cold. Many studies analyse the influence of different system and component parameters on the performance of heat pumps and use exergy analysis to assess the occurrence and distribution of exergy losses and destruction on the component and system side. Most studies on HTHPs are concerned with the provision of process heat with heat sink temperatures below 150°C, and only a few studies focus on heat pump cycles for the simultaneous provision of process heat and cold. However, the upcoming availability of HTHPs with heat supply above 200°C is at an early stage. Therefore, more research should be done on suitable heat pump configurations for the simultaneous provision of process heat and cold with heat sink temperatures above 200°C in order to increase the range of applications and to make the use of heat pumps more attractive for end users.

The present work addresses the research gap of industrial HTHPs with a high-temperature lift for simultaneous provision of process heat above 200°C and process cooling

below 0°C. The work presents a Brayton heat pump cycle with intermediate heating and cooling. The heat pump cycle is simulative designed to achieve a heat sink temperature of 250°C and a heat source temperature in the range of −30°C and 5°C. An exergy analysis is carried out to determine the components with the greatest influence on exergy losses and exergy destruction. A parametric study is carried out to investigate the influence of various parameters on the heat pump performance. To show the advantages and disadvantages with regard to the distribution of exergy in the system, the heat pump cycle is compared to the simple reversed Brayton cycle under the same operating conditions. The investigated heat pump cycles and the thermodynamic models are described. In Section 2, the methods of the modelling and simulation, the exergy analysis and parametric study are explained. Section 3 presents the results of the energy and exergy analysis of both heat pump cycles and the influence of the operating parameters on the heat pump performance followed by a discussion of the results. The last section summarises the relevant results and conclusions. The results of this study provide a better understanding of the advantages and disadvantages of different heat pump cycle configurations for simultaneous heating and cooling with a high-temperature lift and expand the availability of studies on industrial HTHPs. This work can serve as an approach for further design and improvement of existing heat pump cycles, particularly in the industrial sector.

1.2. Heat pump cycle description

Two heat pump cycle configurations based on the reversed closed-loop Brayton cycle are analysed in this work and are presented in Figure 1. In the schematic, the main components of the heat pump cycles are presented as well as the positions of controllers used for the simulation. In both heat pump cycles the turbines and the compressors are mounted on the same shaft to ensure the mechanical power obtained from the turbine is used immediately to partially drive the compressor. Figure 1(a) shows the simple reversed Brayton cycle with recuperation containing a compressor (C), a turbine (T),

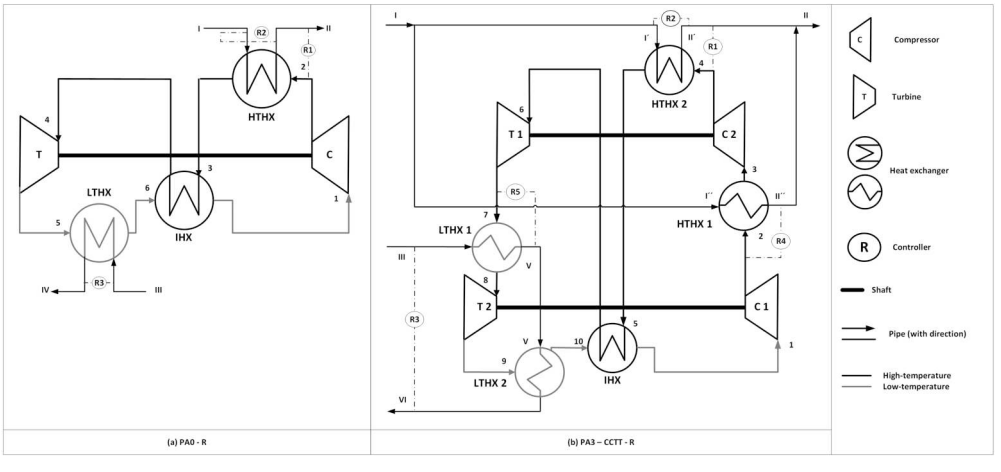

Figure 1. Schematic of the simple reversed, recuperated Brayton heat pump cycle PA0-R (a) and the complex reversed, recuperated Brayton heat pump cycle PA3-CCTT-R (b).

a high-temperature heat exchanger (HTHX), a low-temperature heat exchanger (LTHX) and an internal heat exchanger (IHX). Each reference state point in the system is numbered. Arabic numerals from one to six are used for the primary cycle flows upstream and downstream after each component in the Brayton cycle. The secondary cycle flows at the heat source and the heat sink are numbered with Roman numerals from I to IV. At state point (1), the working fluid is compressed by an electrically operated compressor, leading to an increase of temperature and pressure at state point (2). A heat transfer between the primary and secondary cycles takes place at the high-temperature heat exchanger, with the hot stream transferring heat to the cold stream. Sensible heat $\dot{Q}_{out,sink}$ is transferred to the heat sink (II) and the working fluid in the primary cycle is cooled down. The cooled down working fluid flows in direction to the internal heat exchanger (3), which is used for the recuperation. By flowing through the IHX, the temperature of the working fluid upstream of the turbine (4) is lowered even more by transferring some of the hot residual heat to the working fluid downstream of the IHX, which leads to an increase of the temperature upstream of the compressor (1). The turbine expands the working fluid from (3) to (4) to the initial pressure with a further temperature drop. Downstream the turbine, the working fluid enters the low-temperature heat exchanger (5), where heat $\dot{Q}_{in,source}$ from the heat source (III) is absorbed. Again, the heat transfer between the primary and secondary cycles takes place. After entering the IHX (6), higher temperatures result downstream of the IHX and the compressor (1). When the first state point (1) is reached, the cycle closes and repeats again.

A second heat pump cycle, based on the simple reversed closed-loop Brayton cycle with incorporating several heat exchangers (HX) and turbo machines (TM), representing inter cooled compression and reheated expansion, is shown in Figure 1(b). The complex heat pump cycle includes two compressors (C1) and (C2), two turbines (T1) and (T2), two high-temperature heat exchanger (HTHX1) and (HTHX2), two low-temperature heat exchanger (LTHX1) and (LTHX2) and one internal heat exchanger (IHX). The state points in the primary Brayton cycle are labelled from one to ten, in the secondary cycles from I to V. An inter cooled compression is realised by the integration of an additional heat exchanger at the heat sink (HTHX1) and a reheated expansion is realised by the integration of an additional heat exchanger at the heat source (LTHX1). The secondary cycles of HTHX1 and HTHX2 are connected to each other to ensure one heat sink. The heat sink inlet stream (I) is divided into two equal parts before HTHX1 and HTHX2 to avoid high pressure ratios and mass flows between the compressors. One half of the split heat sink inlet stream flows towards the HTHX1 inlet (I″), realising the cooling of the working medium between the compressors by transferring heat from the hot to the cold stream. The other half of the split heat sink inlet flows towards the HTHX2 inlet (I′), realising the heat transfer to cool the working medium and utilising the sensible heat at the heat sink outlet. The streams downstream of both HTHX are merged, resulting in a single heat sink flow providing potential process heat. On the heat source side, the reheated expansion between the turbines is realised with the LTHX1. The heat source inlet stream (III) of the secondary cycle cools the working medium between the both turbines. The LTHX1 outlet stream (V) serves as the inlet stream of LTHX2. After heat exchange, the cooled down stream leaving the LTHX2 (IV) can be used as possible process cooling.

The cycle configuration in Figure 1(b) was already mentioned in an earlier work by Kabat et al. (2023) and is one of nine heat pump cycles that were investigated for the provision of process heat and cold. This configuration showed the highest COP of all heat pump cycles studied, except the simple Brayton cycle, and performed better than the others, especially at low source temperatures. This cycle was selected for further investigation in this study to compare it with the simple Brayton cycle from an energetic and exergetic point of view to find out what leads to the better performance at cold temperatures and to examine the advantages and disadvantages of such a heat pump cycle.

In order to better distinguish between the two heat pump cycles in the present work, a nomenclature is established. The simple, recuperated Brayton cycle in Figure 1(a) is labelled PA0-R. The novel heat pump cycle in Figure 1(b) is referred to as PA3-CCTT-R. The nomenclature consists of two parts. The first part refers to the designation process architecture labelled PA with an additional number. The second part refers to the number of main components contained in the respective cycle, whereby C stands for a compressor, T for a turbine and R for recuperation. The nomenclature of the investigated cycles is presented in Table 1.

1.3. Heat pump cycle thermodynamics

Figure 2 presents the temperature – entropy (T-s) diagram of an ideal reversed Brayton cycle. The T-s diagram describes the temperature-related changes in state of the working medium, with the temperature on the y-axis being plotted over the respective specific entropy on the x-axis. The working medium is compressed isentropically from state 1 to state 2, which results in an increase in both pressure and temperature. The sensible heat $\dot{Q}_{out,sink}$ is released at constant pressure via a heat exchanger at the heat sink, while the specific entropy decreases from state 2 to 3. The working medium is then expanded isentropically by the turbine from state 3 to 4, which results in a drop in temperature and pressure. The heat source absorbs sensible heat $\dot{Q}_{in,source}$ from the environment isobarically, causing the specific entropy to increase from state 4 to 1. The T-s diagrams resulting from the simulations for the two heat pump cycles presented are shown and discussed in Section 3.1.

The efficiency of a heat pump system, also known as the coefficient of performance (COP), can be calculated according to:

$$COP = \frac{\dot{Q}_{out,sink}}{P} = \frac{\dot{Q}_{out,sink}}{P_C - P_T} \tag{1}$$

by using the ratio of the heat delivered at the heat sink compared to the input power for the compression of the working medium (Arpagaus 2019). $\dot{Q}_{out,sink}$ indicates the heat flow

Table 1. Nomenclature of the heat pump cycles.

	Number of components in the heat pump cycle				
Nomenclature	C	T	HTHX	LTHX	IHX
PA0-R	1	1	1	1	1
PA3-CCTT-R	2	2	2	2	1

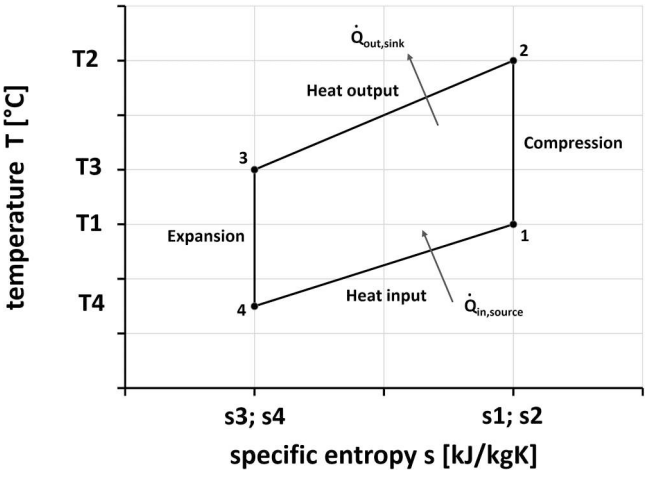

Figure 2. T-s diagram of the ideal reversed Brayton cycle.

delivered at the heat sink and P is the drive power applied to the system, which results from the difference between the power of the compressor P_C and the turbine P_T. The total COP for the simultaneous generation of process heat and cooling also takes into account the thermal input at the heat source $\dot{Q}_{in,source}$:

$$COP_{total} = \frac{\dot{Q}_{out,sink} + \dot{Q}_{in,source}}{P_C - P_T} \tag{2}$$

The thermal heat flow $\dot{Q}$ is expressed by the mass flow $\dot{m}$ and the specific input and output enthalpies h:

$$\dot{Q} = \dot{m} \cdot (h_{out} - h_{in}) = \dot{m} \cdot \Delta h \tag{3}$$

The calculation method using the specific enthalpies takes into account thermodynamic effects such as temperature and pressure changes. The calculation equations for each component can be found in Table A1 in Appendix. In this study, the temperature lift ΔT_{Lift} is considered as the temperature difference between the heat sink outlet temperature and the heat source inlet temperature (Baehr and Kabelac 2016):

$$\Delta T_{Lift} = T_{sink,out} - T_{source,in} = T_{II} - T_{III} \tag{4}$$

The thermodynamic logarithmic mean temperature difference (LMTD) ΔT_m indicates the average temperature that is reached in a heat exchanger when heat is absorbed or released at a non-constant temperature. The LMTD is calculated using the temperature differences of the hot and cold side fluid at the respective inlet and outlet of the heat exchangers (VDI 2013):

$$\Delta T_m = \frac{(T_{hot,in} - T_{cold,out}) - (T_{hot,out} - T_{cold,in})}{ln\dfrac{(T_{hot,in} - T_{cold,out})}{(T_{hot,out} - T_{cold,in})}} \tag{5}$$

2. Methods

This section presents the methods used for examining the two described heat pump cycles. A schematic flowchart of the below described methodology is presented in Figure 3. The modelling and simulation method is described and the component and operating parameters used for the simulation are presented. Based on the simulation results, an energetic and exergetic analysis is carried out followed by a parameter analysis.

2.1. Modelling of the heat pump cycles

The modelling and simulation of the two presented heat pump cycles is carried out with the software tool EBSILON® Professional (EBSILON) version 16.0 (Iqony Ebsilon 2023). EBSILON includes a customisable design component library for cycle process calculation and can visualise energy and mass balances as well as thermodynamic parameters of a process. The simulation is performed in the EBSILON design mode, which means that each cycle with the set boundary conditions represents a fixed designed heat pump system. The components are set up for each cycle and connected to each other as can be seen in the flowchart in Figure 1. The following assumptions are made for the simulations:

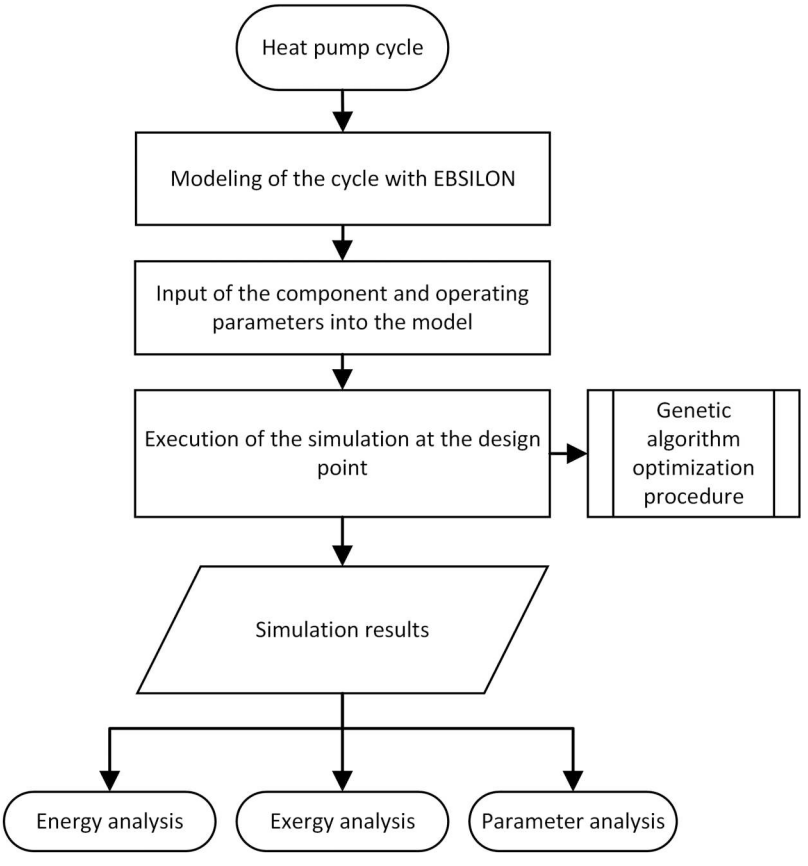

Figure 3. Methodology flowchart.

(1) Steady state conditions
(2) Pressure losses over pipes are neglected
(3) Expansion and compression processes are adiabatic
(4) Calculation of the heat exchangers is conducted via fixed effectiveness
(5) Fixed isentropic efficiencies for turbo machines

The basic assumptions in this work such as the working medium, the heat exchanger effectiveness and the isentropic efficiencies of the turbo machines are made on the basis of an existing DLR heat pump demonstrator (Jende et al. 2022) called 'CoBra'. The heat pump demonstrator is based on the simple recuperated Brayton cycle shown in Figure 1(a) and therefore serves as a reference for the component values in this work. The investigations in this work are based on a fixed defined stationary operating point. Air is used as the working medium in the primary as well as in the secondary cycles because it is environmentally friendly and freely available. As an ideal gas, air shows no critical behaviour with a critical temperature of −118°C for the defined area of investigation. For other working fluids, such as CO_2, the critical temperature is higher around 31°C (Institut für Arbeitsschutz der Deutschen Gesetzlichen Unfallversicherung n.d.). In supercritical CO_2 cycles, the minimum process temperature has a decisive influence on density ratios and thus on the system efficiency (Hacks 2023). Therefore, the choice of working fluid in connection with the minimum process temperature plays a design-relevant role. In the case of air as the working fluid, generalised results can be obtained, which, however, do not necessarily apply to other working fluids. Other working fluids will not be investigated further in this work. The system and component parameters valid for both heat pump cycles are given in Table 2 and described as follows.

It is assumed a small heat pump with a fixed thermal output $\dot{Q}_{out,sink}$ of 150 kWth at the heat sink. The thermal output refers to the scale of an existing DLR heat pump demonstrator (Jende et al. 2022). The temperature assumptions for the heat sink and heat source are based on common requirements for industrial processes in the food industry. In particular, high temperatures above 200°C are required in the food and beverage industry, e.g. as process heat for baking processes and low temperatures in the range from −15°C to −40°C are required for product cooling and freezing (PBL Netherlands Environmental Assessment Agency 2020; Schulz 2014). Therefore, a temperature T_{II} of 250°C at the heat sink and a temperature T_{IV} of −30°C at the heat source is specified to provide process heat and process cooling simultaneously. The inlet

Table 2. System and component parameters of PA0-R and PA3-CCTT-R.

	Symbol	Value
System parameter		
Heat sink heat flow	$\dot{Q}_{out,sink}$	150 kW_{th}
Heat sink inlet temperature	T_I	100°C
Heat sink outlet temperature	T_{II}	250°C
Heat source inlet temperature	T_{III}	60°C
Heat source outlet temperature	T_{IV}	−30°C
Temperature lift	ΔT_{Lift}	190K
Component parameter		
Compressor isentropic efficiency	η_C	0.75
Turbine isentropic efficiency	η_T	0.85
Heat exchanger effectiveness	ε_{HX}	0.9

temperatures of the heat sink and the heat source are based on assumed industrial waste heat sources, which are mainly in the range of 40°C to 100°C (Marina et al. 2021). It is assumed that the inlet temperature of the heat sink T_I is 100°C and the inlet temperature of the heat source T_{III} is 60°C. The resulting temperature lift ΔT_{Lift} is 190 K. The heat exchangers are counter flow heat exchangers with a constant heat exchanger effectiveness of 0.9. Since the calculation is carried out for a fixed design case, the assumption of a fixed heat exchanger effectiveness with common values is sufficiently accurate (Sohel Murshed and Matos Lopes 2017). The compressors and the turbines are simulated with fixed isentropic efficiencies. The compressor and turbine isentropic efficiencies specify the amount of irreversibility due to the deviation from a reversible, ideal process (Dybe, Tanneberger, and Stathopoulos 2019). A constant compressor isentropic efficiency of 0.75 and a constant turbine isentropic efficiency of 0.85 is assumed for the simulations based on the DLR heat pump demonstrator component values.

2.2. Simulation of the heat pump cycles

The fixed temperature specifications for T_{II} and T_{IV} as well as the fixed specification of the heat sink heat flow are implemented by a control system. A control unit or controller in EBSILON is used to set operating conditions in a targeted manner. The controller in the system takes action when a specific control variable in the system is to keep a specific target value. If the specified target value differs from the actual value of the control variable, the controller takes action by changing the so-called actuating variable. The positions of the controllers in both cycles are marked with R in Figure 1. The control and actuating variables as well as the control limits for each controller are presented in Table 3.

Three controllers are used in the simple and five in the complex heat pump cycle. Controller R1 is used to set a fixed heat sink outlet temperature of 250°C by varying the pressure in the range between 2 and 25 bar downstream of the compressor for the cycle PA0-R and between 3 and 25 bar downstream of the compressor C2 for the cycle PA3-CCTT-R. Controller R2 is used to set a fixed thermal output at the heat sink to the target value of 150 kW by varying the heat sink mass flow in the range from 0.3 to 2 kg/s. Controller R3 sets the heat source outlet temperature to −30°C by varying the heat source mass flow in the range of 1–2 kg/s. Controller R4 sets the heat sink outlet temperature of the intermediate cooling through the HTHX1 to 250°C by varying the outlet pressure of compressor C1 in the range from 1.5–25 bar. Controller R5 regulates the temperature between the heat source heat exchangers LTHX1 and LTHX2 in the range of 15°C and 60°C via the outlet pressure of turbine T1, which is varied between 1.2 and 25 bar. The limit of 60°C is chosen to not exceed the heat source inlet temperature. After setting the fixed system and component parameters as

Table 3. Control parameter used for the simulation of PA0-R and PA3-CCTT-R.

Controller	Control variable	Target Value	Actuating variable	Limits	PA0-R	PA3-CCTT-R
R1	T_{II}	250°C	Pressure (after C)	2–25bar (abs)	x	
R1	$T_{II'}$	250°C	Pressure (after C2)	3–25bar (abs)		x
R2	$\dot{Q}_{out,sink}$	150kWth	Heat sink mass flow	0.3–2 kg/s	x	x
R3	T_{IV}	−30°C	Heat source mass flow	0.1–2 kg/s	x	x
R4	$T_{II''}$	250°C	Pressure (after C1)	1.5–25bar (abs)		x
R5	T_V	15–60°C	Pressure (after T1)	1.2–25bar (abs)		x

well as the controller variables, the simulation is carried out in EBSILON design mode using the internal optimiser EbsOptimize (Iqony Ebsilon 2023). EbsOptimize is used to optimise a specification value through parameter variation in a given value range to optimise the target value. The specification values that are optimised in this work are the initial mass flow of the primary cycle in front of the first compressor C and C1 at state point 1 for both cycles and the outlet temperature T_V of the LTHX1 which is controlled by R5. The target value for the optimisation of these two values is the maximisation of the total COP. The optimisation is performed on the basis of a genetic algorithm (GA) with a constant population size and convergence as the termination criterion. The genetic algorithm procedure is presented in Figure 4. The genetic algorithm parameters are illustrated in Table 4 and are based on the standard parameters from EBSILON for using the genetic algorithm (Iqony Ebsilon 2025). The genetic algorithm starts with initialising the population of the first generation for each of the two values. The population contains a set of random values in the given value range. The best value is chosen and selected for the next generation. The crossover and mutation probability ensure that more possible solution values are generated. The results of the first population are then used as the value set for the next population. The algorithm runs through the procedure until it has reached the number of specified generations and the convergence criterion (Rooker 1991). The simulation is carried out for both cycles for heat source outlet temperatures between −30 and +5°C in 5°C steps. After setting the heat source outlet temperature T_{IV} via controller R4 to a target value, the simulation including the optimisation procedure starts. In both cycle configurations, the mass flow of the primary cycle is varied in the range from 0.3 to 1 kg/s to maximise the total COP. Additionally, the

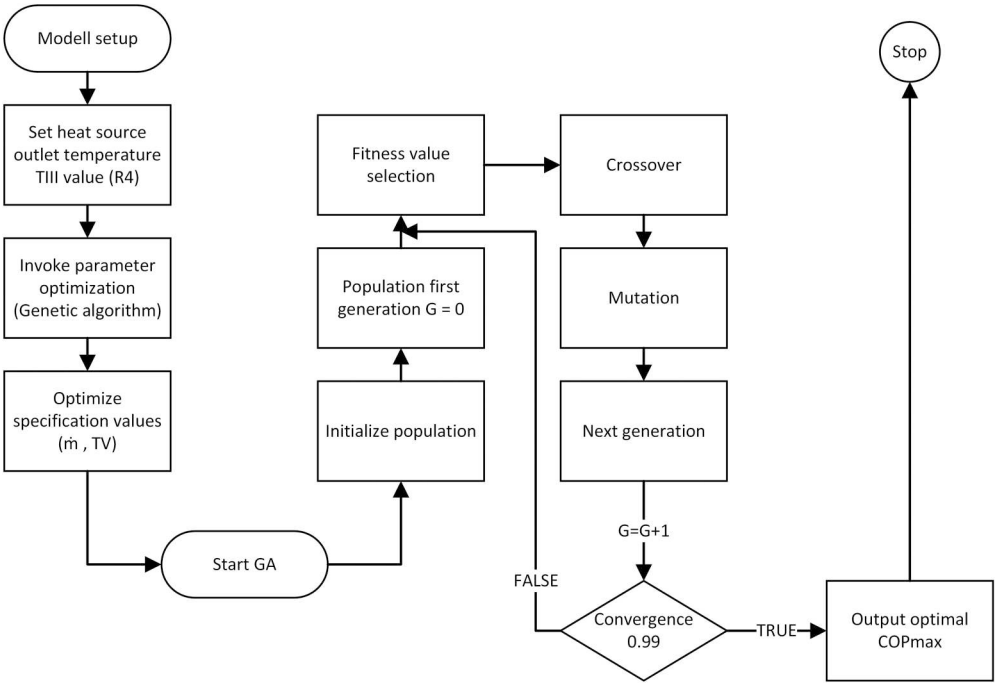

Figure 4. Flowchart of the genetic algorithm optimisation procedure.

Table 4. Genetic algorithm parameters for optimisation.

Parameter	Value
Population size	15
Generation size	500
Crossover probability	0.6
Mutation function	0.5
Convergence	0.99

temperature T_V in the complex cycle PA3-CCTT-R is varied in the range of 15°C and 60° C to maximise the total COP.

After applying the defined operating and boundary conditions in the simulation model, the parameters for temperature, pressure, mass flow, specific enthalpy and specific exergy are calculated by the simulation for each numbered state point in the cycle.

2.3. Exergy analysis

An exergy analysis of the two presented cycle configurations is carried out to evaluate the exergy loss and destruction due to heat and mechanical losses of the systems. Kotas (1985) describes the exergy analysis as a suitable method for characterising the quality of energy and for localising exergy losses in order to visualise the optimisation potential of heat pump components. Exergy is defined as the maximum work that can be obtained from a thermodynamic system. In this study, the exergy flow is used and referred to as exergy $\dot{E}x$ (Kotas 1985):

$$\dot{E}x = \dot{E}x_k + \dot{E}x_p + \dot{E}x_{ph} + \dot{E}x_{ch} \tag{6}$$

$$\dot{E}x = \dot{m} \cdot ex \tag{7}$$

Assuming that the kinetic exergy $\dot{Ex}_{k,}$ the potential exergy $\dot{Ex}_p$ and the chemical exergy $\dot{Ex}_{ch}$ are negligible in this work, the physical exergy $\dot{Ex}_{ph}$ results in the specific physical exergy ex given by Eq. 8 (Kotas 1985):

$$ex = (h - h_0) - T_0(s - s_0) \tag{8}$$

with the specific physical exergy ex, the specific enthalpy h and the specific entropy s. For the reference state, the temperature, the specific enthalpy and the specific entropy is given by T_0, h_0 and s_0. The specific enthalpies, specific entropies and the resulting specific exergy for each state point, are calculated using the software EBSILON version 16.0 (Iqony Ebsilon 2023). The physical properties for calculating the specific enthalpies and entropies are based on the gas and material value tables of the FDBR (Fachverband Dampfkessel-, Behalter- und Rohrleitungsbau) for air under real gas assumption. The reference temperature T_0 and the reference pressure p_0 is set to $T_0 = 273.15$ K and $p_0 = 1.01325$ bar. While exergy indicates the maximum work potential of a specific type of energy, a certain amount of exergy is lost in a process due to irreversibilities (Kotas 1985):

$$\Delta\dot{E}x_{loss} = T_0 \cdot \Delta\dot{S}$$

The exergy loss flow $\Delta\dot{E}x_{\mathrm{loss}}$ results from the entropy production flow $\Delta\dot{S}$ at the thermodynamic reference temperature T_0. Exergy losses occur as a result of heat losses to the environment or as a result of mechanical losses in turbo machinery. In addition, exergy

destruction can occur through heat transfer with finite temperature differences in heat exchangers or through entropy generation in turbo machinery (von Böckh and Stripf 2015). In this work, the term exergy loss is used throughout, but refers to the exergy lost due to exergy losses and exergy destruction. Based on the exergy balance for an adiabatic control region with steady state conditions, the total exergy loss $\Delta\dot{E}x_{\text{lost}}$ due to exergy losses and destruction is as follows (Kotas 1985):

$$\dot{E}x_{lost} = \dot{E}x_{in} - \dot{E}x_{out} + \dot{E}x_{Work}$$

The total exergy loss $\dot{E}x_{\text{lost}}$ due to irreversibilities is therefore only due to the change in exergy caused by mass flows $\dot{E}x_{in}$ and $\dot{E}x_{out}$ and work $\dot{E}x_{Work}$. For adiabatic compressors, turbines and heat exchangers the exergy loss is calculated as given below (Kotas 1985):

$$\dot{E}x_{lost,C} = \dot{E}x_{in} - \dot{E}x_{out} + P_C$$

$$\dot{E}x_{lost,T} = \dot{E}x_{in} - \dot{E}x_{out} - P_T$$

$$\dot{E}x_{lost,HX} = \Delta\dot{E}x_{hot} - \Delta\dot{E}x_{cold} = (\dot{E}x_{in,hot} - \dot{E}x_{out,hot}) - (\dot{E}x_{out,cold} - \dot{E}x_{in,cold})$$

For the heat exchangers, $\Delta\dot{E}x_{hot}$ is defined as the temperature difference of the hot stream and $\Delta\dot{E}x_{cold}$ as the temperature difference of the cold stream. With the given equations, the total exergy losses of the simple Brayton cycle PA0-R and the complex Brayton cycle PA3-CCTT-R can be calculated as follows:

$$\dot{E}x_{lost,PA0-R} = \dot{E}x_{lost,C} + \dot{E}x_{lost,HTHX} + \dot{E}x_{lost,T} + \dot{E}x_{lost,LTHX} + \dot{E}x_{lost,IHX}$$

$$\begin{aligned}\dot{E}x_{lost,PA3-CCTT-R} = {} & \dot{E}x_{lost,C1} + \dot{E}x_{lost,C2} + \dot{E}x_{lost,HTHX1} + \dot{E}x_{lost,HTHX2} + \dot{E}x_{lost,T1} \\ & + \dot{E}x_{lost,T2} + \dot{E}x_{lost,LTHX1} + \dot{E}x_{lost,LTHX2} + \dot{E}x_{lost,IHX}\end{aligned}$$

The exergy loss can be used to calculate the exergy efficiency Ψ of a component which serves as a performance criterion. The exergy efficiency rates the quality with which the available exergy is utilised. The exergy or so-called rational efficiency is the ratio of the desired exergy output to the exergy input. The exergy efficiencies of the turbo machines and the heat exchangers are calculated as follows (Kotas 1985):

$$\Psi_C = \frac{\dot{E}x_{out} - \dot{E}x_{in}}{P_C} = 1 - \frac{\dot{E}x_{lost,C}}{P_C}$$

$$\Psi_T = \frac{P_T}{\dot{E}x_{in} - \dot{E}x_{out}} = 1 - \frac{\dot{E}x_{lost,T}}{\dot{E}x_{in} - \dot{E}x_{out}}$$

$$\Psi_{HX} = \frac{\dot{E}x_{out,cold} - \dot{E}x_{in,cold}}{\dot{E}x_{in,hot} - \dot{E}x_{out,hot}} = 1 - \frac{\dot{E}x_{lost,HX}}{\dot{E}x_{in,hot} - \dot{E}x_{out,hot}}$$

The relative irreversibility I is used to relate the exergy loss of a component to the total exergy loss of the heat pump system. The component with the highest irreversibility rate also shows the greatest potential for improvement (Kotas 1985):

$$I = \frac{\dot{E}x_{lost,component}}{\dot{E}x_{lost,system}}$$

Besides the COP, the exergetic efficiency η_{ex} takes into account the exergy losses that occur in the system and can be used as a further criterion of performance:

$$\eta_{ex} = \frac{\dot{E}x_{sink} + \dot{E}x_{source}}{P} = \frac{P_{el,system} - \dot{E}x_{d,tot}}{P_{el,system}}$$

The exergy balances, exergetic efficiencies and relative irreversibilities are calculated according to the equations given in Table A1 in Appendix for each component of the cycles.

2.4. Parameter analysis

A parametric study is carried out for the complex heat pump cycle PA3-CCTT-R to evaluate the impact of different parameters on the heat pump performance. The influence of the isentropic efficiency of the compressors and turbines, the effectiveness of the heat exchangers and the heat sink and heat source inlet temperatures on the total COP of the heat pump cycle is investigated. Table 5 presents the variation of the parameters with the initial values and the range of the parameter variation. The isentropic efficiencies of the compressors and turbines are varied in 5% increments, the heat exchanger effectiveness in 2% increments, the heat sink inlet temperature in 20% and the heat source inlet temperature in 10% increments starting from the initial value. All parameters, except those whose influence is being analysed, are kept constant. The parametric study is carried out at the fixed operating point described in Table 2.

3. Results

In this section, the resulting T-s diagrams of the two heat pump cycles are presented. The performance of both cycles is discussed and the influence of the heat source outlet temperature on the total COP is shown. The results of the exergy analysis carried out for both cycles for a defined operating point at −30°C heat source outlet temperature and 250°C heat sink outlet temperature are presented and compared. The exergy losses of the system and the components are analysed. Finally, the results of the parametric study for the complex heat pump cycle are shown.

Table 5. Variation of parameters for the parametric study of PA3-CCTT-R.

Parameter	Component	Initial value	Parameter range
isentropic efficiency η_C	C1; C2	0.75	0.6–0.9
isentropic efficiency η_T	T1; T2	0.85	0.75–0.95
heat exchanger effectiveness ε_{HX}	HTHX1; HTHX2; LTHX1; LTHX2; IHX	0.9	0.84–0.96
heat sink inlet temperature T_I	heat sink inlet	100°C	40–120°C
heat source inlet temperature T_{III}	heat source inlet temperature; temperature lift	60°C; 190K	42–72°C; 178–208K

3.1. T-s diagrams

The resulting T-s diagrams for each cycle are presented in Figures 5 and 6, respectively. The diagrams are based on the simulative obtained temperature and specific entropy values for each state point in the described operating point.

Figure 5 presents the T-s diagram for the simple reversed and recuperated Brayton cycle PA0-R. The compression takes places from state point (1) to (2) followed by the heat output from (2) to (3) over the HTHX at the heat sink. From state point (3) to (4), the internal heat transfer trough the recuperation by the IHX can be seen, followed by the expansion through the turbine from (4) to (5). The heat input from the heat source by the LTHX can be seen from (5) to (6). After another internal heat exchange by the IHX, the cycle is closed from (6) to (1). In Figure 6, the T-s diagram of the complex Brayton cycle PA3-CCTT-R is presented. Due to the inter cooled compression and reheated expansion, the diagram shows two compression stages from (1) to (2) and from (3) to (4) as well as two expansion stages from (6) to (7) and (8) to (9). While both compressors perform approximately the same compression work, it can be clearly seen from the expansion curves that the first turbine T1, in contrast to the second turbine T2, performs hardly any work. The heat output via the respective HTHX1 and HTHX2 takes place from (2) to (3) and from (4) to (5). The heat input from the heat source via LTHX1 and LTHX2 takes place from (7) to (8) and (9) to (10). It can be seen that the heat input via LTHX1 is lower than via LTHX2. The internal heat transfer through the IHX is described by the changes of state from (5) to (6) and (10) to (1). Since both heat pump cycles are non-ideal cycles, no isentropic changes take place. Irreversibilities are taken into account at the turbo machinery by means of the isentropic efficiency and at the heat exchangers by means of the effectiveness. A first comparison of the two cycles using the T-s diagram shows that the inter cooled compression makes sense in terms of avoiding excessively high, non-usable temperatures. Furthermore, it can be seen that there is an imbalance in the work distribution of the two turbines, especially at the heat source with turbine T1 showing little advantage under the given simulation conditions.

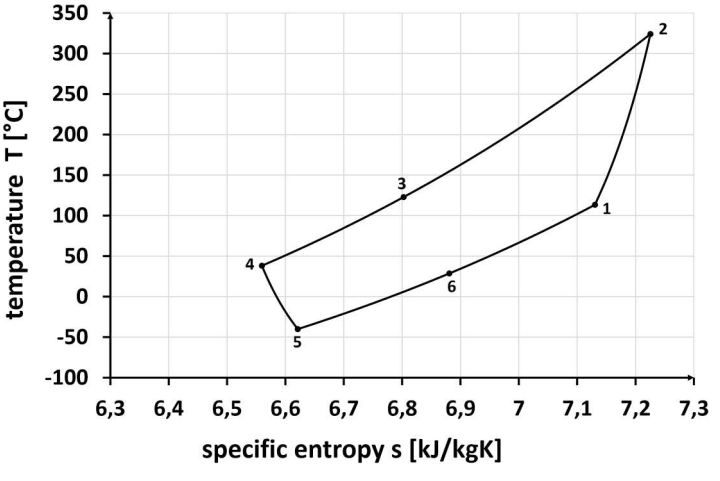

Figure 5. T-s diagram of the simple recuperated Brayton cycle PA0-R.

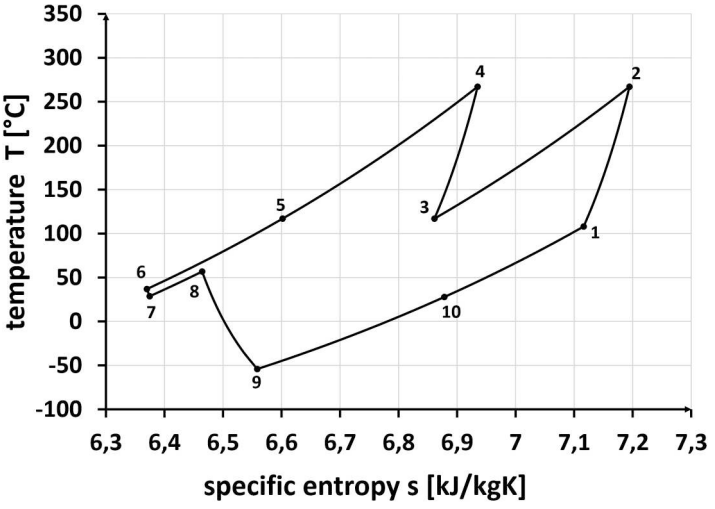

Figure 6. T-s diagram of the complex recuperated Brayton cycle PA3-CCTT-R.

3.2. Cycle performance and COP

Table 6 shows the mechanical P_{mech} and thermal $\dot{Q}_{th}$ power consumption as well as the pressure ratio of the turbo machines for both cycles. It can be seen, that the mechanical power consumption of the complex Brayton cycle configuration is lower than for the simple cycle. By intercooling the compression and re-heating the expansion, the compression and expansion process can be carried out more efficiently due to smaller temperature differences over the turbo machine stages. Irreversibilities due to high temperature differences are reduced, which in turn leads to less necessary compression or expansion work. By that, lower pressure ratios occur in the turbo machinery for the inter cooled and reheated cycle, since temperature differences per compression or expansion are reduced and thus a more efficient energy conversion takes place. The difference

Table 6. Mechanical and thermal performance data for $T_{IV} = -30°C$.

Component	P_{mech} (kW)	$\dot{Q}_{th}$ (kW*th*)	Π
PA0-R			
C	158.59	157.08	3.395
T	−56.39	−62.42	3.395
HTHX		150.07	
LTHX		49.98	
IHX		62.42	
Σ	102.2		
PA3-CCTT-R			
C1	80.23	79.43	2.639
T2	−53.87	−54.42	5.834
C2	75.76	75	2.469
T1	−3.98	−4.02	1.117
HTHX1		75	
HTHX2		75	
LTHX1		13.8	
LTHX2		40.20	
IHX		39.44	
Σ	98.14		

between the mechanical and thermal power in the compressor and turbine reflects losses, e.g. due to friction and heat losses. Due to idealised assumptions for the simulation, the deviation of the mechanical from the thermal power is only very small. In a real application, losses due to mechanical friction, internal leakage, heat loss to the environment and inefficiencies in energy transfer would also have to be taken into account, which would in the end affect the performance of the heat pump. In general, the results show a positive influence of the inter cooled compression and reheated expansion on the cycle performance. Nevertheless, it can be seen that the turbine T1 only generates a small amount of mechanical work. The heat transfer at the first heat source heat exchanger LTHX1 also transfers a low heat output. Both indicate that the reheated expansion process is not optimally designed and would need to be adapted. In the case of a technical realisation of the complex cycle, it is questionable whether turbine T1 and heat exchanger LTHX1 should be used under the given conditions, since no great energetic gain in terms of economic efficiency can be achieved.

In Figure 7, the total COP of both cycles is displayed against the variation of the heat source outlet temperature in the range of −30°C up to +15°C. The simulation results for the COP values are compared with the data published in Kabat et al. (2023) for validation purposes. Each data point represents an independent design point of the heat pump configuration. The COP values determined in this work are slightly smaller from the comparative data in Kabat et al. (2023), which is due to a modified simulation algorithm with convergence as a termination criterion and a higher number of generations. The components and operating parameters are the same in both studies, which explains the good approximation of the values. For the complex Brayton cycle PA3-CCTT-R a total COP of 2.08 and for the simple Brayton cycle PA0-R a total COP of 1.96 is achieved

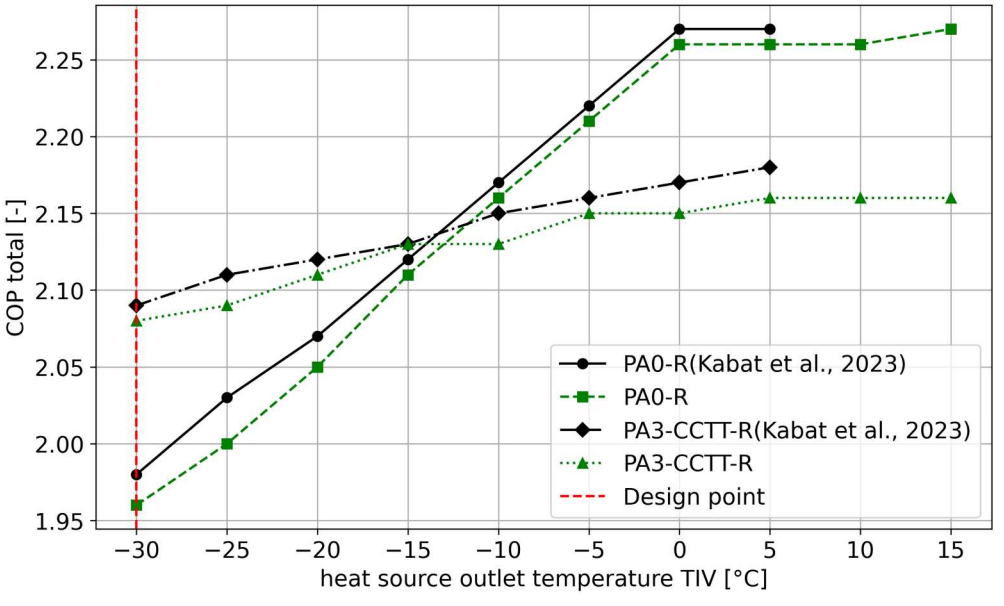

Figure 7. Comparison of the total COP for different heat source outlet temperatures calculated in this work with published data from Kabat et al. (2023).

for the design point in the present study. The complex cycle with inter cooled compression and reheated expansion is more efficient than the simple Brayton cycle at temperatures below −13°C. This is due to less mechanical power required by the turbo machine, which has an inversely proportional effect on the COP according to Equation (2). In general, the COP is increasing with higher heat source outlet temperature for both cycles. The COP of both cycles intersects at −13°C with a total COP of 2.14. After the intersection, the total COP of the simple cycle remains higher than that of the complex one for the investigated temperature range.

3.3. Exergy analysis

The exergy analysis is carried out for both heat pump cycles at a fixed design point for a heat source outlet temperature of −30°C. The resulting temperature, pressure, mass flow, specific enthalpy, specific exergy, enthalpy flow and exergy flow for each state point in the system is presented in Table A2 in Appendix. The resulting exergy loss, exergy efficiency, relative irreversibility of each component, and the exergetic efficiency of the entire system are shown in Table 7. The exergy analysis reveals that in the complex cycle PA3-CCTT-R, fewer exergy losses occur in the system via the components, which leads to a better exergetic efficiency of the cycle. The simple Brayton cycle PA0-R has an exergetic efficiency of 54.4%, the complex one of 56.4%. The largest exergy losses in the simple cycle occur at the compressor, resulting in a relative irreversibility of about 44%. This means that the compressor in this cycle has the greatest potential for improvement in terms of optimising exergy losses and exergy destruction. In the complex cycle, the turbine T2 has the highest relative irreversibility with 30.6%. Overall, the complex cycle shows an increase in the exergetic efficiency of 2% compared to the simple cycle due to the introduction of inter cooled compression and reheated expansion.

Table 7. Exergy loss, exergy efficiency and relative irreversibility of components.

	$\dot{E}x_{lost}$ (kW)	Ψ / η_{ex} (%)	I (%)
PA0-R			
C	20.34	87.2	43.6
T	12.74	81.6	27.3
Σ	33.08		
HTHX	8.58	87.1	18.4
LTHX	3.61	63	7.7
IHX	1.36	90.3	2.9
Σ	46.63	54.4	100
PA3-CCTT-R			
C1	11.23	86	26.2
T2	13.09	80.5	30.6
Σ	24.32		
C2	10.58	86	24.7
T1	0.68	85.3	1.6
Σ	11.26		
HTHX1	1.72	94.4	4
HTHX2	1.72	94.4	4
LTHX1	0.22	89.5	0.5
LTHX2	2.71	13.2	6.3
IHX	0.82	90.3	1.9
Σ	42.77	56.4	100

Figure 8 presents the summed up exergy lost in the components of both cycles. With a total of 42.8 kW, the complex cycle shows less exergy loss in the system than the simple cycle with 46.6 kW. The lower exergy losses resulting from the modified process control through inter cooled compression and reheated expansion lead to the complex Brayton cycle having a higher COP than the simple cycle at the operating point under investigation. Due to the idealised assumptions, however, higher exergy losses of the components should be expected in reality for both cycles. The highest exergy losses occur in the turbo machinery in both cycles. The compressors in total cause most of the exergy losses of the turbo machines in both cycle configurations, representing around 61% of the system exergy losses. Due to the lower isentropic efficiency of the compressors in contrast to the turbines, higher losses occur at the compressors, since the process is less close to ideal. The doubled number of turbo machines in the complex cycle leads to a higher amount of irreversibilities on the components and results in higher losses than in a simple cycle. The exergy losses at the heat exchangers in the complex cycle, especially at the HTHX are significantly lower due to a split heat demand than in the simple cycle, so that these offset the higher exergy losses via the turbo machinery. In the simple cycle, the largest losses in relation to all heat exchangers occur at the high-temperature heat exchangers. Due to inter cooled compression in the complex cycle, the losses at the HTHX are significantly reduced because the hot stream of the HTHXs has significantly lower temperatures than in the simple cycle. The temperatures at the inlet of the HTHX are significantly influenced by the highest total pressure ratio in the system, which is set to achieve the specified temperature boundary conditions at the heat sink and source. For the simple cycle, lower total pressure ratio in the system occur than in the complex cycle. However, the intercooling of the compression leads to lower temperatures behind each compressor stage, which means that the total temperature increase due to the

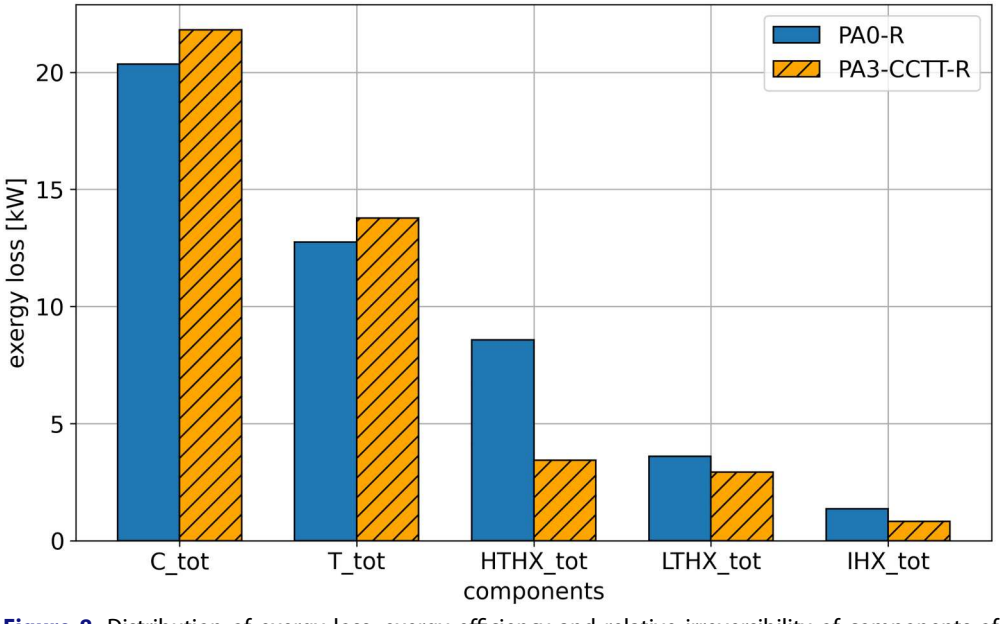

Figure 8. Distribution of exergy loss, exergy efficiency and relative irreversibility of components of PA3-CCTT-R.

compression is lower. Accordingly, a lower HTHX inlet temperature can be achieved despite the high total pressure ratio. This reduces both the required mechanical energy and thus the exergy losses that occur.

The influence of the different inlet temperatures at the heat exchangers in both cycles affecting the logarithmic mean temperature difference can be seen in Table A3 in Appendix. Overall, the inter cooled compression has a positive influence on the temperature distribution in the system, which leads to fewer entropy production and exergy losses at the heat sink side. In contrast, the exergy losses of the LTHXs at the heat source side are approximately the same for both cycles. Due to the fact that the turbine T1 performs only a small amount of mechanical work, the effectiveness of the first heat source heat exchanger LTHX1 is also impaired. Two-stage expansion with reheating does not work effectively under the given simulation conditions and provide only a small advantage in terms of reducing exergy losses. The component-related distribution of exergy loss, exergy efficiency and relative irreversibility of the complex cycle PA3-CCTT-R is presented in Figure 9. The corresponding diagram for the simple cycle PA0-R can be found in Figure A1 in Appendix.

Approximately equal exergy losses occur at the two compressor stages C1 and C2. Due to a slightly greater temperature difference of 8 K in the compressor stage C1, it has to perform more compression work, which leads to higher exergy losses. It is noticeable that the highest exergy losses in the system occur at turbine T2, due to a high pressure

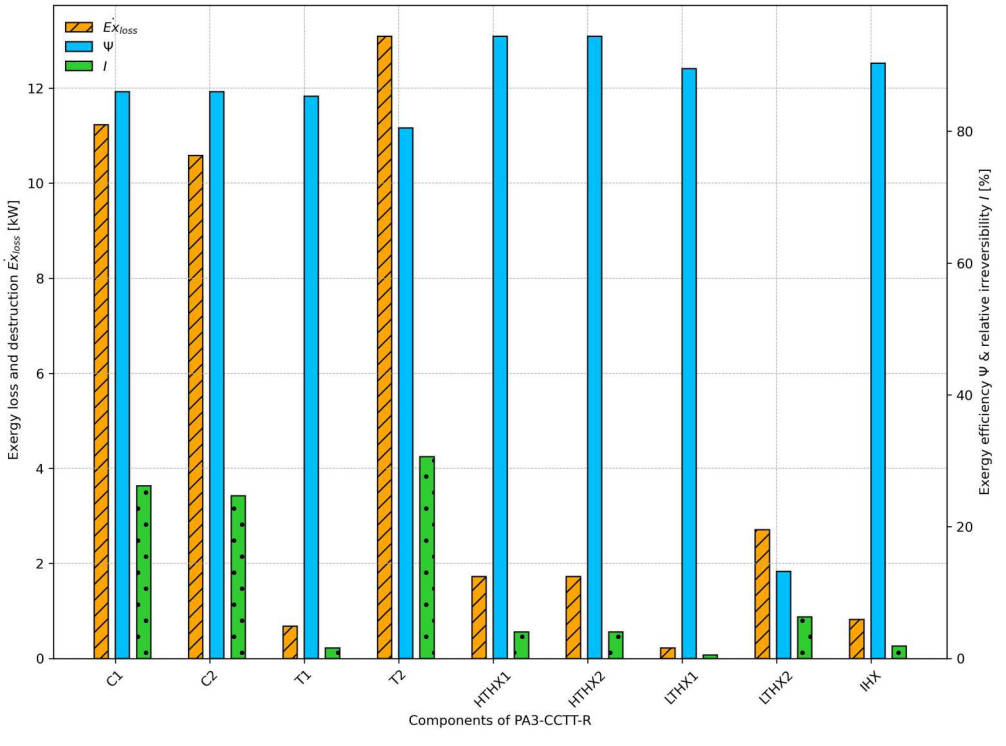

Figure 9. Distribution of exergy loss, exergy efficiency and relative irreversibility of components of PA3-CCTT-R.

ratio needed at this turbine for the expansion to the desired temperature at the heat source outlet. In contrast, only minor exergy losses occur at turbine T1, since this turbine performs almost no mechanical work due to a very low pressure ratio. The low pressure ratio in turbine T1 and the high pressure ratio in turbine T2 strongly shift the expansion work and the exergy losses towards turbine T2, which leads to an inefficient use of exergy. Controlling the temperature T_V via controller R5 is the cause of the low pressure ratio of turbine T1. As described in the chapter simulation in Table 3, the temperature T_V of the secondary cycle at the LTHX1 is controlled via the outlet pressure of the first turbine. The maximum temperature limit of 60°C seems to be not sufficient to set a sufficiently high pressure ratio at the turbine. The low specific work of the first turbine associated with this is a direct consequence of the temperature control in the reheated expansion. Since the temperature of the stream after the limited expansion in turbine T1 is only slightly below the temperature T_V of the secondary stream of the LTHX1, the heat output of this heat exchanger, is also very low. Due to the small temperature difference between the primary and secondary cycles, hardly any heat can be transferred resulting in minor entropy production and less exergy losses. An equal distribution of exergy losses occurs at the high-temperature heat exchangers of the heat sink. This is reasoned by the distribution of the heat sink inlet flow and the subsequent merging of the heat sink outlet flow of the two heat exchangers HTHX1 and HTHX2. The split heat sink inlet stream halves the heat sink mass flow and thus the heat consumption for each heat exchanger to 75 kW. The advantages of an internal heat exchanger are evident in the efficient heat transfer from the hot to the cold side of the heat pump cycle with minor exergy losses.

The results of the comparison of the component-related exergy losses for the simple and complex heat pump cycle shows that the arrangement and application of multi-stage compression and expansion has a significant influence on the overall pressure ratio in the system. The arrangement of the secondary heat sink cycle leads to a reduction in exergy losses at the heat exchangers, especially at the high-temperature heat exchangers. By that, an overall performance improvement for simultaneous heating and cooling can be achieved.

3.4. Parametric study

The results of the parametric study of the complex cycle PA3-CCTT-R are presented in this section. The influence of the isentropic efficiency of the compressors and turbines, the effectiveness of the heat exchangers and the heat sink and heat source inlet temperature on the total COP of the heat pump cycle is analysed. Furthermore, the influence of the heat sink and heat source inlet temperature on the total COP are investigated.

3.4.1. Influence of isentropic efficiency

Figure 10 shows the effect of the variation of the compressor and turbine isentropic efficiency η on the total COP of the complex cycle PA3-CCTT-R. The total COP of the system is plotted against the isentropic efficiency of the turbo machinery. The isentropic efficiency of the compressors is varied between 0.6 and 0.9 with 0.75 as the starting point and the isentropic efficiency for both turbines is varied between 0.75 and 0.95 based on the initial value of 0.85. In general, a higher isentropic efficiency leads to a higher total

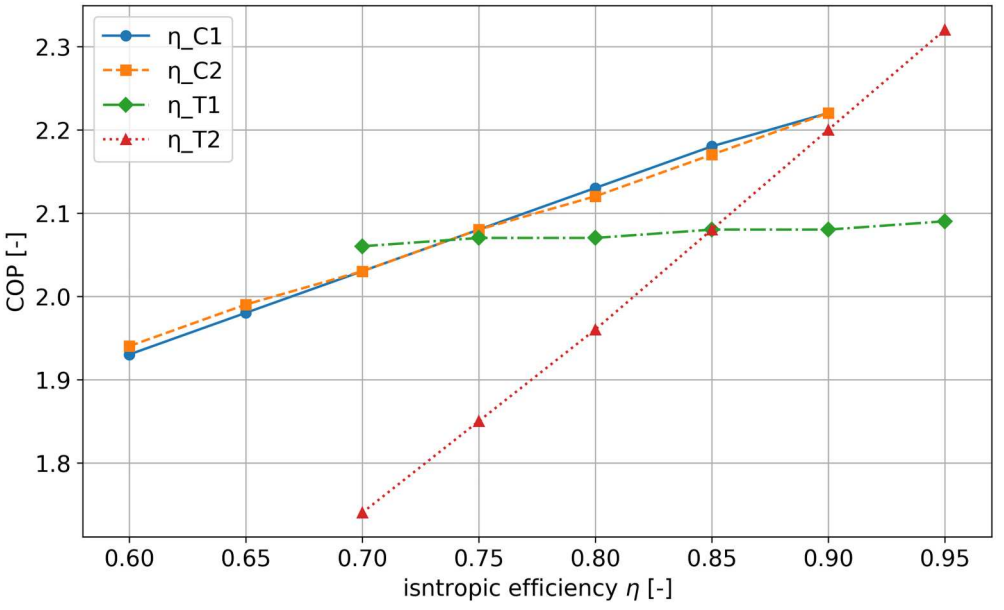

Figure 10. Influence of the compressor and turbine isentropic efficiency on the total COP of PA3-CCTT-R.

COP of the system due to a smaller deviation from the ideal process and lower entropy generation during the compression and expansion process. Owing to the split heat sink, a nearly even distribution of the compression work performed results and the influence of the variation of η_{C1} and η_{C2} on the total COP is almost the same. The different trends for the variation of η_T results from the different expansion work performed by the turbines. Only minor work is performed on turbine T1 thus, the improvement in the efficiency of T1 has only a minor influence on the total COP due to the smaller amount of energy converted by this turbine in contrast to T2. The total COP of the system can be improved mainly by increasing the isentropic efficiency of the turbo machinery that operates most of the work, in this case turbine T2. A change in the isentropic efficiency of a particular component mainly affects the entropy production and the resulting component-related exergy losses, and only has a minor effect on the entropy production of other components.

3.4.2. Influence of heat exchanger effectiveness

Figure 11 presents the effect of the variation of the heat exchanger effectiveness ε on the total COP of the complex cycle PA3-CCTT-R. The total COP of the system is plotted against the heat exchanger effectiveness varying between 0.84 and 0.96 with 0.9 as the starting value for the parameter variation. The effectiveness of the IHX could only be increased to 0.94, since at 0.96 the desired thermal heat sink flow of 150 kW could not be achieved under the given conditions. The intersection of the graphs indicates the total COP of the system at the described design point. In general, an increasing heat exchanger effectiveness leads to a higher total COP of the system. Increasing the effectiveness of a heat exchanger leads to improved heat

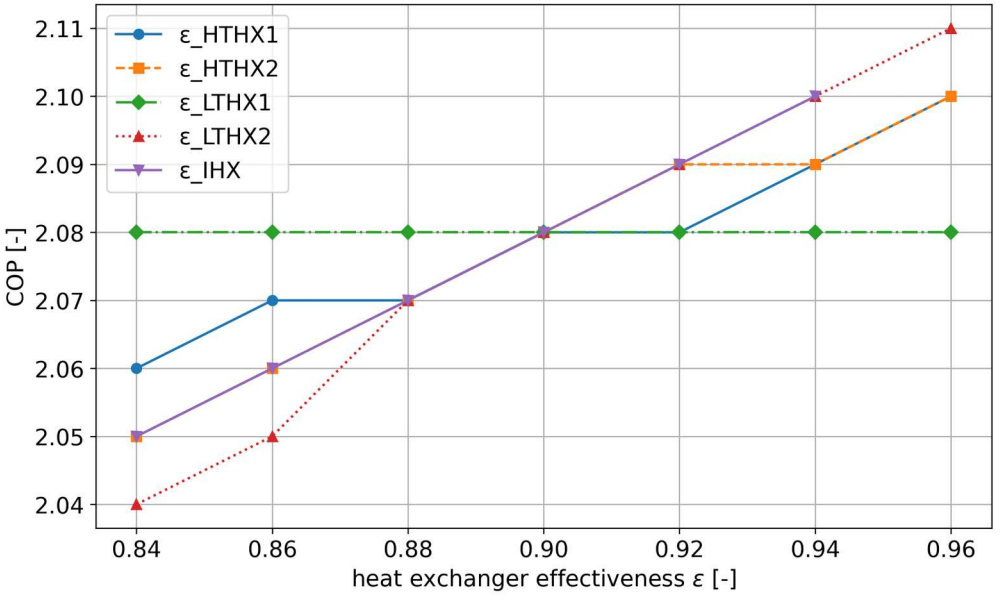

Figure 11. Influence of the heat exchanger effectiveness on the total COP of PA3-CCTT-R.

transfer from the hot stream to the cold stream, resulting in lower entropy production during the heat transfer and thus lower exergy losses and an improvement in the total COP of the system. Due to the minor thermal heat transfer at the LTHX1, an improvement in the heat exchanger effectiveness has no significant influence on the total COP of the system. The logarithmic mean temperature difference of the LTHX1 indicates a very low driving temperature difference between the primary and secondary sides. This limits the amount of heat that can be transferred and leads to an inefficient operating point. Overall, the total COP of the system can be improved mainly by increasing the effectiveness of the heat exchanger. The heat exchanger that transfers the greatest thermal power, in this case the LTHX2, has the greatest influence on the total COP of the overall system.

3.4.3. Influence of the temperature lift

Figure 12 displays the influence of the temperature lift ΔT_{Lift} on the total COP of the complex system PA3-CCTT-R. The variation of the heat source inlet temperature T_{III} between 42°C and 72°C results in a temperature lift between 208 and 178 K. The temperature lift for the design point is 190 K with a COP of 2.08. It can be seen that the total COP of the system is decreasing with an increasing temperature lift. With increasing temperature lift, more mechanical energy is required to transport the heat across the temperature gradient. A maximum total COP of 2.12 is obtained for the lowest temperature lift at 178 K. A minimum total COP of 1.98 results for the highest temperature lift at 208 K. An analysis of the component-related exergy losses reveals that the exergy loss increases with increasing temperature lift on the heat source side for LTHX2 and T2. Due to the higher temperature level during expansion and heat transfer, more exergy is lost through irreversible processes.

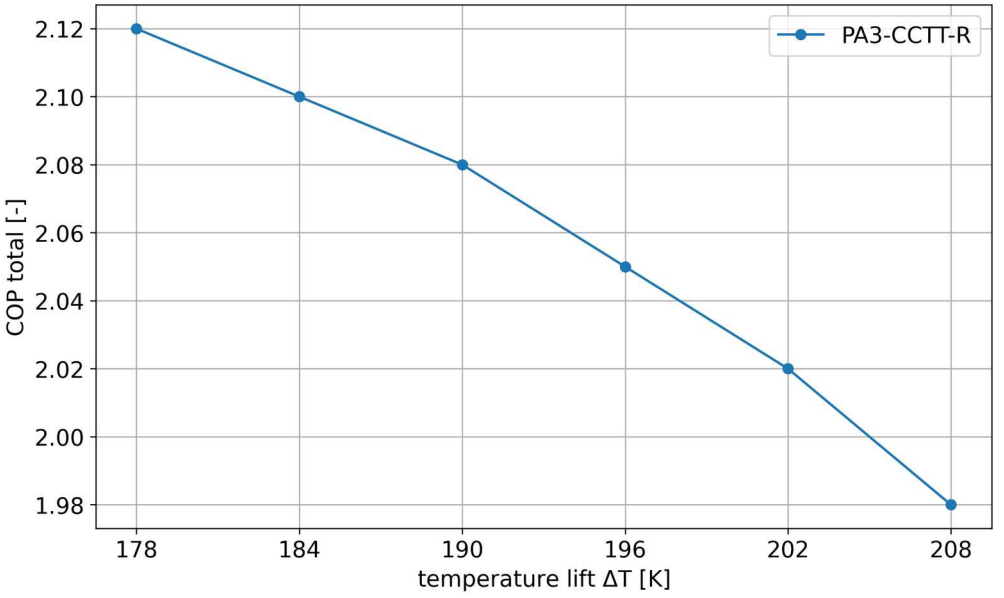

Figure 12. Influence of the temperature lift on the total COP of PA3-CCTT-R.

3.4.4. Influence of heat sink inlet temperature

Figure 13 illustrates the influence of the heat sink inlet temperature T_I on the total COP of the complex cycle PA3-CCTT-R. The total COP is displayed against the heat sink inlet temperature in the range of 40°C and 160°C. An increasing T_I leads to a decreasing total COP. A maximum total COP of 2.14 and a minimum total COP of 1.91 results for the variation. A higher inlet temperature at the heat sink requires that the fluid on the hot side of the heat sink heat exchangers be compressed to a higher temperature in order to obtain an adequate temperature gradient for the heat transfer. However, due to the increased exergy of the transferred heat, increasing losses also occur due to irreversibilities at the heat exchangers, which ultimately leads to a reduced system performance.

4. Discussion

The exergetic analysis of the complex cycle PA3-CCTT-R shows that intercooling and reheating can achieve a moderate increase in the COP from 1.96 to 2.08. In particular, at heat source temperatures below −13°C, the complex cycle achieves better efficiency than the simple cycle by better matching the temperature curves during compression and expansion. The efficiency increase is due to improved exergy utilisation as a result of reduced irreversible losses in the system. However, when it comes to the practical implementation of this cycle, the relatively small performance gain is offset by increased design and control complexity. The additional components increase both capital and maintenance costs. A system with inter cooled compression and reheated expansion increases the heat pump efficiency, but a decision should be made based on the specific process application as to whether such a system makes sense. In general, the simple Brayton cycle offers a sufficiently high-performance efficiency for applications

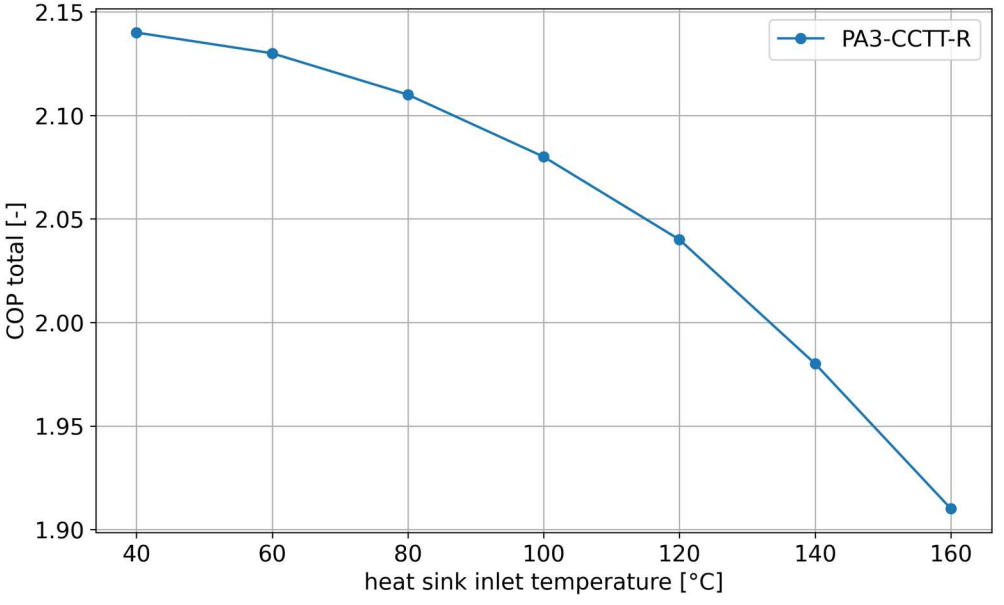

Figure 13. Influence of the heat sink inlet temperature on total COP of PA3-CCTT-R.

that provide process heating and cooling, with simple construction and control. The modelling and simulation of the cycles in this work is based on partially idealised assumptions that simplify an energetic and exergetic evaluation but limit the transferability of the results to real systems. In the practical implementation, especially of the complex cycle, further loss mechanisms occur that can lead to a deviation in system performance. Assuming air as the working medium, the minimum process temperature of −54°C is not in the critical range and can therefore be used as a generalised assumption for possible technical implementations. However, for other working media, such as CO_2, this temperature is well below the critical point and therefore does not allow any conclusion to be drawn about the feasibility of supercritical CO_2 power systems. The results of this work and the conclusions drawn from it provide a theoretical basis on which realistic and cost-based assessments can be built in further studies. In further work, the actual properties of the components and performance characteristics, as well as loss mechanisms such as pressure losses, partial load behaviour and environmental influences, should be taken into account. A techno-economic analysis should include investment and operating costs, as well as the complexity of control in relation to efficiency gains to analyse an assessment of practical feasibility. An experimental validation of the presented system is not part of this work, since a technical realisation of the presented complex cycle does not yet exist. An experimental validation of the Brayton cycle is planned for further studies with the DLR heat pump demonstrator.

5. Conclusions

In this study, a thermodynamic analysis of two heat pump cycles based on the reversed and recuperated Brayton cycle for the simultaneous provision of process heat at 250°C

and process cooling at −30°C was carried out. The simple Brayton cycle was compared to a complex Brayton cycle with inter cooled compression and reheated expansion. Both cycles are compared by using an exergy analysis. Furthermore, a parametric study for the complex cycle investigating the influence of isentropic efficiency, effectiveness and heat sink and source temperature on the total COP was performed.

Both heat pump cycles are capable for achieving the desired temperatures of the heat sink and the heat source under the given conditions. Due to inter cooled compression and reheated expansion, the complex Brayton cycle shows an improved exergetic efficiency as a result of reduced irreversible losses by improved temperature profiles leading to a better exergy utilisation during the compression and expansion processes. The complex Brayton cycle achieves a total COP of 2.08, while the simple Brayton cycle achieves 1.96. In the complex cycle, most of the exergy loss and destruction occurs at the turbo machines, which is why they offer the greatest potential for optimisation to increase efficiency. Through appropriate heat sink and source distribution, losses due to irreversibilities can be reduced, mainly at the heat exchangers. The results show that the systematic arrangement of the components has a decisive influence on the pressure and temperature distribution in the cycle. Improper design of the process streams and control strategies can have a thermodynamically ineffective influence on components. A holistic analysis of the cycle can reveal disproportionate effects and lead to an optimised exergetic use in the system. Heat pump cycles with intercooling and heating can be particularly advantageous if high pressure ratios are required in the process, different process temperatures have to be provided or very low temperatures have to be provided at the heat source. The simple Brayton cycle offers sufficiently high efficiency for low-pressure-ratio applications and for simultaneous provision of process heat and cooling with low heat source outlet temperatures. However, the decision as to whether the increased performance achieved is economically viable should be carefully considered. The present work contributes to the analysis and evaluation of complex Brayton cycles with integrated intermediate cooling and heating, whereby the provision of process heat and cold takes place simultaneously at a high-temperature lift. The results can serve as a basis for future work by considering a techno-economic analysis with realistic and cost-based evaluations, real operating conditions or alternative working fluids.

Disclosure statement

No potential conflict of interest was reported by the author(s).

Data availability statement

All data used in this study are available upon request.

References

Adamson, K.-M., T. G. Walmsley, J. K. Carson, Q. Chen, F. Schlosser, L. Kong, and D. J. Cleland. 2022. "High-Temperature and Transcritical Heat Pump Cycles and Advancements: A Review." *Renewable and Sustainable Energy Reviews* 167:112798. https://doi.org/10.1016/j.rser.2022.112798.

Ahmed, M. M., and M. M. Ehsan. 2023. "Design and off-Design Performance Analysis of a Zigzag Channeled Precooler for Indirect Cooling System of Supercritical CO_2 Recompression Cycle Incorporated with a Flow-Bypass System." *Applied Thermal Engineering* 226:120321. https://doi.org/10.1016/j.applthermaleng.2023.120321.

Ahrens, M. U., S. S. Foslie, O. M. Moen, M. Bantle, and T. M. Eikevik. 2021. "Integrated High Temperature Heat Pumps and Thermal Storage Tanks for Combined Heating and Cooling in the Industry." *Applied Thermal Engineering* 189:116731. https://doi.org/10.1016/j.applthermaleng.2021.116731.

Angelino, G., and C. Invernizzi. 1995. "Prospects for Real-Gas Reversed Brayton Cycle Heat Pumps." *International Journal of Refrigeration* 18 (4): 272–280. https://doi.org/10.1016/0140-7007(95)00005-V.

Arpagaus, C. 2019. *Hochtemperatur-Wärmepumpen: Marktübersicht, Stand der Technik und Anwendungspotenziale, Neuerscheinung Edition*. Berlin/Offenbach: VDE Verlag GmbH. https://www.content-select.com/index.php?id=bib_view&ean=9783800745517.

Arpagaus, C., F. Bless, M. Uhlmann, J. Schiffmann, and S. S. Bertsch. 2018. "High Temperature Heat Pumps: Market Overview, State of the art, Research Status, Refrigerants, and Application Potentials." *Energy* 152:985–1010. https://doi.org/10.1016/j.energy.2018.03.166.

Arunwattana, W. 2022. "Heat Pump Design for Simultaneous Cooling Space and Heating Water Coupled with Earth-Tube Heat Exchanger as Secondary Heat Sink." *Trends in Sciences* 19:2899. https://www.semanticscholar.org/paper/Heat-Pump-Design-for-Simultaneous-Cooling-Space-andArunwattana/78a2c037dffe5bac667a9a2b1cf6b09e0ea5fddf.

Ayou, D. S., R. Hargiyanto, and A. Coronas. 2022. "Ammonia-based Compression Heat Pumps for Simultaneous Heating and Cooling Applications in Milk Pasteurization Processes: Performance Evaluation." *Applied Thermal Engineering* 217:119168. https://doi.org/10.1016/j.applthermaleng.2022.119168.

Baehr, H. D., and S. Kabelac. 2016. *Thermodynamik: Grundlagen und Technische Anwendungen*. 16th ed. Berlin/Heidelberg: Springer. https://nbn-resolving.org/urn:nbn:de:bsz:31-epflicht-1486485.

Bataille, C., M. Åhman, K. Neuhoff, L. J. Nilsson, M. Fischedick, S. Lechtenböhmer, B. Solano-Rodriquez, et al. 2018. "A Review of Technology and Policy Deep Decarbonization Pathway Options for Making Energy-Intensive Industry Production Consistent with the Paris Agreement." *Journal of Cleaner Production* 187:960–973. https://doi.org/10.1016/j.jclepro.2018.03.107.

Byrne, P., and R. Ghoubali. 2019. "Exergy Analysis of Heat Pumps for Simultaneous Heating and Cooling." *Applied Thermal Engineering* 149:414–424. https://doi.org/10.1016/j.applthermaleng.2018.12.069.

Dai, B., X. Liu, S. Liu, Y. Zhang, D. Zhong, Y. Feng, V. Nian, and Y. Hao. 2020. "Dual-pressure Condensation High Temperature Heat Pump System for Waste Heat Recovery: Energetic and Exergetic Assessment." *Energy Conversion and Management* 218:112997. https://doi.org/10.1016/j.enconman.2020.112997.

Dumont, M., R. Wang, D. Wenzke, K. Blok, and R. Heijungs. 2023. "The Techno-Economic Integrability of High-Temperature Heat Pumps for Decarbonizing Process Heat in the Food and Beverages Industry." *Resources, Conservation and Recycling* 188:106605. https://doi.org/10.1016/j.resconrec.2022.106605.

Dybe, S., T. Tanneberger, and P. Stathopoulos. 2019. "Second Law Analysis of an Energy Storage System Consisting of an Electrolysis Plant and the Graz Cycle with Internal H_2/O_2 Combustion." ASME Turbo Expo 2019: Turbomachinery Technical Conference and Exposition.

Ehsan, M. M., M. Awais, S. Lee, S. Salehin, Z. Guan, and H. Gurgenci. 2023. "Potential Prospects of Supercritical CO_2 Power Cycles for Commercialisation: Applicability, Research Status, and Advancement." *Renewable and Sustainable Energy Reviews* 172:113044. https://doi.org/10.1016/j.rser.2022.113044.

Ehsan, M. M., S. Duniam, Z. Guan, H. Gurgenci, and A. Klimenko. 2019. "Seasonal Variation on the Performance of the dry Cooled Supercritical CO_2 Recompression Cycle." *Energy Conversion and Management* 197:111865. https://doi.org/10.1016/j.enconman.2019.111865.

Ehsan, M. M., S. Duniam, J. Li, Z. Guan, H. Gurgenci, and A. Klimenko. 2019. "Effect of Cooling System Design on the Performance of the Recompression CO_2 Cycle for Concentrated Solar Power Application." *Energy* 180:480–494. https://doi.org/10.1016/j.energy.2019.05.108.

Ehsan, M. M., S. Duniam, J. Li, Z. Guan, H. Gurgenci, and A. Klimenko. 2020. "A Comprehensive Thermal Assessment of dry Cooled Supercritical CO_2 Power Cycles." *Applied Thermal Engineering* 166:114645. https://doi.org/10.1016/j.applthermaleng.2019.114645.

Ehsan, M. M., Z. Guan, H. Gurgenci, and A. Klimenko. 2020. "Feasibility of Dry Cooling in Supercritical CO_2 Power Cycle in Concentrated Solar Power Application: Review and a Case Study." *Renewable and Sustainable Energy Reviews* 132:110055. https://doi.org/10.1016/j.rser.2020.110055.

Ehsan, M. M., Z. Guan, H. Gurgenci, and A. Klimenko. 2020. "Novel Design Measures for Optimizing the Yearlong Performance of a Concentrating Solar Thermal Power Plant Using Thermal Storage and a Dry-Cooled Supercritical CO_2 Power Block." *Energy Conversion and Management* 216:112980. https://doi.org/10.1016/j.enconman.2020.112980.

Ehsan, M. M., Z. Guan, and A. Y. Klimenko. 2018. "A Comprehensive Review on Heat Transfer and Pressure Drop Characteristics and Correlations with Supercritical co 2 under Heating and Cooling Applications." *Renewable and Sustainable Energy Reviews* 92:658–675. https://doi.org/10.1016/j.rser.2018.04.106.

Ehsan, M. M., Z. Guan, A. Y. Klimenko, and X. Wang. 2018. "Design and Comparison of Direct and Indirect Cooling System for 25 MW Solar Power Plant Operated with Supercritical CO_2 Cycle." *Energy Conversion and Management* 168:611–628. https://doi.org/10.1016/j.enconman.2018.04.072.

Ehsan, M. M., X. Wang, Z. Guan, and A. Y. Klimenko. 2018. "Design and Performance Study of Dry Cooling System for 25 MW Solar Power Plant Operated with Supercritical CO_2 Cycle." *International Journal of Thermal Sciences* 132:398–410. https://doi.org/10.1016/j.ijthermalsci.2018.06.024.

Gai, L., P. S. Varbanov, T. G. Walmsley, and J. J. Klemes. 2020. "Critical Analysis of Process Integration Options for Joule-Cycle and Conventional Heat Pumps." *Energies* 13 (3): 635. https://doi.org/10.3390/en13030635.

Gao, J. T., Z. Y. Xu, and R. Z. Wang. 2021. "An air-Source Hybrid Absorption-Compression Heat Pump with Large Temperature Lift." *Applied Energy* 291:116810. https://doi.org/10.1016/j.apenergy.2021.116810.

Hacks, A. J. 2023. "Untersuchung zur Auslegungsmethodik von sCO2-Kreisläufen in Abhängigkeit von Verdichter- und Kreislaufauslegungsparametern." Ph.D. diss., DuEPublico: Duisburg-Essen Publications Online, University of Duisburg-Essen.

Heat Pumping Technologies. 2022. *Annex 58, Task 1 – Technologies – Annex 58*. Accessed December 19, 2022. https://heatpumpingtechnologies.org/annex58/task1/.

IEA. 2022. *The Future of Heat Pumps – Analysis*. Paris: IEA. Accessed February 12, 2024. https://www.iea.org/reports/the-future-of-heat-pumps.

IEA. 2023. *CO_2 Emissions in 2022 – Analysis*. Paris: IEA. Accessed February 15, 2024. https://www.iea.org/reports/co2-emissions-in-2022.

IEA. 2024. *Industry – Energy System*. Paris: IEA. Accessed November 11, 2024. https://www.iea.org/energy-system/industry#tracking.

Institut für Arbeitsschutz der Deutschen Gesetzlichen Unfallversicherung. n.d. Gestis Substance Database. Accessed November 6, 2024. https://gestis.dguv.de/.

Iqony Ebsilon. 2023. https://www.ebsilon.com/de/.

Iqony Ebsilon. 2025. *Ebsilon®Professional Online Dokumentation: Optimierung*. Accessed March 19, 2025. https://help.ebsilon.com/DE/Optimierung.html.

Jende, E., N. Kabat, P. Stathopoulos, and E. Nicke. 2023. "Thermodynamic Analysis of an Industrial Process Integration of a Reversed Brayton High-Temperature Heat Pump: A Case Study of an Industrial Food Process." *E3S Web of Conferences* 414:03006. https://doi.org/10.1051/e3sconf/202341403006.

Jende, E., L. Schleuss, J. Oehler, and E. Nicke. 2022. "Entwicklung und Aufbau von Hochtemperatur-Wärmepumpen zur Integration regenerativer Energieträger in industrielle Prozesse und thermische Speicherkraftwerke." In *Kraftwerkstechnik 2022, Kraftwerkstechnik*, edited by M. Beckmann, 225–236. Freiberg: Innovation- und Kreislaufwirtschaft Sachsen e.V. https://elib.dlr.de/190490/.

Kabat, N., E. Jende, E. Nicke, and P. Stathopoulos. 2023. "Investigation on Process Architectures for High-Temperature Heat Pumps Based on a Reversed Brayton Cycle." ASME Turbo Expo 2023: Turbomachinery Technical Conference and Exposition. https://asmedigitalcollection.asme.org/GT/proceedings/GT2023/86984/V005T06A015/1168025?searchresult=1.

Kabat, N., J. Oehler, and P. Stathopoulos. 2025. "Experimental Exergy Analysis of a High-Temperature Brayton Heat Pump." ASME Turbo Expo 2025: Turbomachinery Technical Conference and Exposition.

Kosmadakis, G. 2019. "Estimating the Potential of Industrial (High-Temperature) Heat Pumps for Exploiting Waste Heat in eu Industries." *Applied Thermal Engineering* 156:287–298. https://doi.org/10.1016/j.applthermaleng.2019.04.082.

Kotas, T. J. 1985. *The Exergy Method of Thermal Plant Analysis*. London: Butterworths.

Marchionni, M., G. Bianchi, and S. A. Tassou. 2018. "Techno-Economic Assessment of Joule-Brayton Cycle Architectures for Heat to Power Conversion from High-Grade Heat Sources Using CO_2 in the Supercritical State." *Energy* 148:1140–1152. https://doi.org/10.1016/j.energy.2018.02.005.

Marina, A., S. Spoelstra, H. A. Zondag, and A. K. Wemmers. 2021. "An Estimation of the European Industrial Heat Pump Market Potential." *Renewable and Sustainable Energy Reviews* 139:110545. https://doi.org/10.1016/j.rser.2020.110545.

Mateu-Royo, C., J. Navarro-Esbrı, A. Mota-Babiloni, M. Amat-Albuixech, and F. Moles. 2018. "Theoretical Evaluation of Different Hightemperature Heat Pump Configurations for low-Grade Waste Heat Recovery." *International Journal of Refrigeration* 90:229–237. https://doi.org/10.1016/j.ijrefrig.2018.04.017.

Mateu-Royo, C., J. Navarro-Esbrı, A. Mota-Babiloni, F. Moles, and M. Amat-Albuixech. 2019. "Experimental Exergy and Energy Analysis of a Novel High-Temperature Heat Pump with Scroll Compressor for Waste Heat Recovery." *Applied Energy* 253:113504. https://doi.org/10.1016/j.apenergy.2019.113504.

Padilla, R. V., Y. C. Soo Too, R. Benito, and W. Stein. 2015. "Exergetic Analysis of Supercritical CO_2 Brayton Cycles Integrated with Solar Central Receivers." *Applied Energy* 148:348–365. https://doi.org/10.1016/j.apenergy.2015.03.090.

PBL Netherlands Environmental Assessment Agency. 2020. *Decarbonisation Options for the Dutch Potato Products Industry*. Accessed February 29, 2024. https://www.pbl.nl/en/publications/decarbonisation-options-for-the-dutch-potato-products-industry.

Rehfeldt, M., T. Fleiter, and F. Toro. 2018. "A Bottom-up Estimation of the Heating and Cooling Demand in European Industry." *Energy Efficiency* 11 (5): 1057–1082. https://doi.org/10.1007/s12053-017-9571-y.

Rooker, Terry. 1991. "Review of Genetic Algorithms in Search, Optimization, and Machine Learning." *AI Magazine* 12 (1): 102. https://doi.org/10.1609/aimag.v12i1.889.

Sarkar, J. 2009. "Second law Analysis of Supercritical CO_2 Recompression Brayton Cycle." *Energy* 34 (9): 1172–1178. https://doi.org/10.1016/j.energy.2009.04.030.

Schlosser, F., M. Jesper, J. Vogelsang, T. G. Walmsley, C. Arpagaus, and J. Hesselbach. 2020. "Large-Scale Heat Pumps: Applications, Performance, Economic Feasibility and Industrial Integration." *Renewable and Sustainable Energy Reviews* 133:110219. https://doi.org/10.1016/j.rser.2020.110219.

Schulz, J. 2014. "Leitfaden Energieeffizienz in Bäckereien - Energieeinsparungen in Backstube und Filialen." https://www.selbstaendig-im-handwerk.de/downloads/News/EnEffBaeckerei-Leitfaden-Juli2014.pdf.

Sohel Murshed, S. M., and Manuel Matos Lopes, eds. 2017. *Heat Exchangers*. Rijeka: IntechOpen.

Sun, S., H. Guo, and M. Gong. 2019. "Thermodynamic Analysis of Single-Stage Compression air-Source Heat Pumps with Different Recuperation Ways for Large Temperature Lift." *International Journal of Refrigeration* 108:91–102. https://doi.org/10.1016/j.ijrefrig.2019.09.006.

VDI, e. V., ed. 2013. *VDI-Wärmeatlas [VDI-Buch]*. 11th ed. Berlin/Heidelberg: Springer.

von Böckh, P., and M. Stripf. *Technische Thermodynamik: Ein Beispielorientiertes Einführungsbuch*. 2nd ed. Berlin/Heidelberg: Springer, 2015. https://nbn-resolving.org/urn:nbn:de:bsz:31-epflicht-1488093.

Wolf, V. 2022. "Investigation of sCO_2 Cycle Layouts for the Recovery of Low Temperature Heat Sources." https://sco2symposium.com/proceedings2022/042-paper.pdf.
Wu, J., S. Sun, Q. Song, D. Sun, D. Wang, and J. Li. 2023. "Energy, Exergy, Exergoeconomic and Environmental (4e) Analysis of Cascade Heat Pump, Recuperative Heat Pump and Carbon Dioxide Heat Pump with Different Temperature Lifts." *Renewable Energy* 207:407–421. https://doi.org/10.1016/j.renene.2023.03.028.
Zühlsdorf, B., F. Bühler, M. Bantle, and B. Elmegaard. 2019. "Analysis of Technologies and Potentials for Heat Pump-Based Process Heat Supply above 150°C." *Energy Conversion and Management: X* 2:100011. https://doi.org/10.1016/j.ecmx.2019.100011.

Appendix

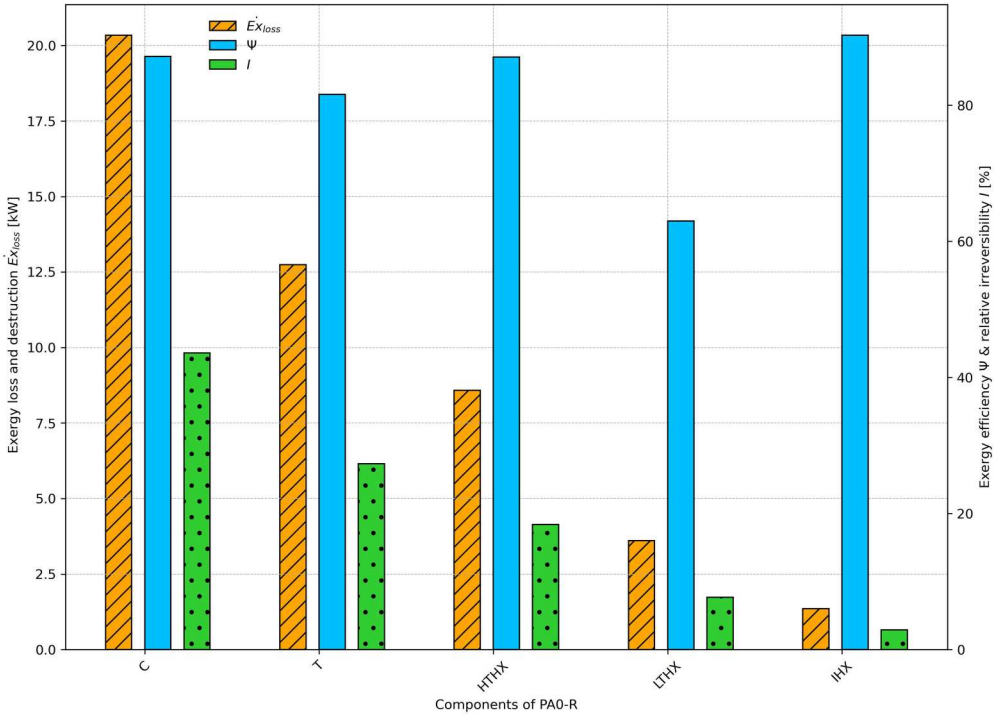

Figure A1. Distribution of exergy loss, exergy efficiency and relative irreversibility of components of PA0-R.

Table A1. Calculation equations of the exergy balances, the exergy efficiency, the relative irreversibility and the thermal heat flows for the components of PA0-R and PA3-CCTT-R.

Component	Exergy balance	Ψ	I	$\dot{Q}_{th}$
PA0-R				
C	$P_C = \dot{Ex}_2 - \dot{Ex}_1 + \dot{Ex}_{lost}$	$= \frac{\dot{Ex}_2 - \dot{Ex}_1}{P_C}$	$= \frac{\dot{Ex}_{lost,C}}{\dot{Ex}_{lost,tot}}$	$= \dot{m}_1 \cdot (h_2 - h_1)$
T	$\dot{Ex}_4 - \dot{Ex}_5 = P_T + \dot{Ex}_{lost}$	$= \frac{P_T}{\dot{Ex}_4 - \dot{Ex}_5}$	$= \frac{\dot{Ex}_{lost,T}}{\dot{Ex}_{lost,tot}}$	$= \dot{m}_3 \cdot (h_4 - h_3)$
HTHX	$\dot{Ex}_2 + \dot{Ex}_I = \dot{Ex}_3 + \dot{Ex}_{II} + \dot{Ex}_{lost}$	$= \frac{\dot{Ex}_{II} - \dot{Ex}_I}{\dot{Ex}_2 - \dot{Ex}_3}$	$= \frac{\dot{Ex}_{lost,HTHX}}{\dot{Ex}_{lost,tot}}$	$= \dot{m}_3 \cdot (h_3 - h_2)$
LTHX	$\dot{Ex}_{III} + \dot{Ex}_5 = \dot{Ex}_{IV} + \dot{Ex}_6 + \dot{Ex}_{lost}$	$= \frac{\dot{Ex}_6 - \dot{Ex}_5}{\dot{Ex}_{III} - \dot{Ex}_{IV}}$	$= \frac{\dot{Ex}_{lost,LTHX}}{\dot{Ex}_{lost,tot}}$	$= \dot{m}_5 \cdot (h_6 - h_5)$
IHX	$\dot{Ex}_{IV} + \dot{Ex}_6 = \dot{Ex}_4 + \dot{Ex}_1 + \dot{Ex}_{lost}$	$= \frac{\dot{Ex}_1 - \dot{Ex}_6}{\dot{Ex}_3 - \dot{Ex}_4}$	$= \frac{\dot{Ex}_{lost,IHX}}{\dot{Ex}_{lost,tot}}$	$= \dot{m}_1 \cdot (h_6 - h_1)$
PA3-CCTT-R				
C1	$P_{C1} = \dot{Ex}_2 - \dot{Ex}_1 + \dot{Ex}_{lost}$	$= \frac{\dot{Ex}_2 - \dot{Ex}_1}{P_{C1}}$	$= \frac{\dot{Ex}_{lost,C1}}{\dot{Ex}_{lost,tot}}$	$= \dot{m}_1 \cdot (h_2 - h_1)$
C2	$P_{C2} = \dot{Ex}_4 - \dot{Ex}_3 + \dot{Ex}_{lost}$	$= \frac{\dot{Ex}_4 - \dot{Ex}_3}{P_{C2}}$	$= \frac{\dot{Ex}_{lost,C2}}{\dot{Ex}_{lost,tot}}$	$= \dot{m}_3 \cdot (h_4 - h_3)$
T1	$\dot{Ex}_6 - \dot{Ex}_7 = P_{T1} + \dot{Ex}_{lost}$	$= \frac{P_{T1}}{\dot{Ex}_6 - \dot{Ex}_7}$	$= \frac{\dot{Ex}_{lost,T1}}{\dot{Ex}_{lost,tot}}$	$= \dot{m}_6 \cdot (h_7 - h_6)$
T2	$\dot{Ex}_8 - \dot{Ex}_9 = P_{T2} + \dot{Ex}_{lost}$	$= \frac{P_{T2}}{\dot{Ex}_8 - \dot{Ex}_9}$	$= \frac{\dot{Ex}_{lost,T2}}{\dot{Ex}_{lost,tot}}$	$= \dot{m}_8 \cdot (h_9 - h_8)$
HTHX1	$\dot{Ex}_2 + \dot{Ex}_{I''} = \dot{Ex}_3 + \dot{Ex}_{II''} + \dot{Ex}_{lost}$	$= \frac{\dot{Ex}_{II''} - \dot{Ex}_{I''}}{\dot{Ex}_2 - \dot{Ex}_3}$	$= \frac{\dot{Ex}_{lost,HTHX1}}{\dot{Ex}_{lost,tot}}$	$= \dot{m}_2 \cdot (h_3 - h_2)$
HTHX2	$\dot{Ex}_4 + \dot{Ex}_{I'} = \dot{Ex}_5 + \dot{Ex}_{II'} + \dot{Ex}_{lost}$	$= \frac{\dot{Ex}_{II'} - \dot{Ex}_{I'}}{\dot{Ex}_4 - \dot{Ex}_5}$	$= \frac{\dot{Ex}_{lost,HTHX2}}{\dot{Ex}_{lost,tot}}$	$= \dot{m}_4 \cdot (h_5 - h_4)$
LTHX1	$\dot{Ex}_7 + \dot{Ex}_{III} = \dot{Ex}_8 + \dot{Ex}_V + \dot{Ex}_{lost}$	$= \frac{\dot{Ex}_8 - \dot{Ex}_7}{\dot{Ex}_{III} - \dot{Ex}_V}$	$= \frac{\dot{Ex}_{lost,LTHX1}}{\dot{Ex}_{lost,tot}}$	$= \dot{m}_7 \cdot (h_8 - h_7)$
LTHX2	$\dot{Ex}_V + \dot{Ex}_9 = \dot{Ex}_{IV} + \dot{Ex}_{10} + \dot{Ex}_{lost}$	$= \frac{\dot{Ex}_{10} - \dot{Ex}_9}{\dot{Ex}_V - \dot{Ex}_{IV}}$	$= \frac{\dot{Ex}_{lost,LTHX2}}{\dot{Ex}_{lost,tot}}$	$= \dot{m}_9 \cdot (h_{10} - h_9)$
IHX	$\dot{Ex}_5 + \dot{Ex}_{10} = \dot{Ex}_6 + \dot{Ex}_1 + \dot{Ex}_{lost}$	$= \frac{\dot{Ex}_1 - \dot{Ex}_{10}}{\dot{Ex}_5 - \dot{Ex}_6}$	$= \frac{\dot{Ex}_{lost,IHX}}{\dot{Ex}_{lost,tot}}$	$= \dot{m}_1 \cdot (h_{10} - h_1)$

Table A2. Thermodynamic parameters at a heat source outlet temperature of −30°C for PA0-R and PA3-CCTT-R.

No.	T (°C)	p (bar_g)	h (kJ/kg)	$\dot{H}$(kW)	ex (kJ/kg)	$\dot{Ex}$ (kW)	$\dot{m}$ (kg/s)
PA0-R							
1	113	1	114.085	83.054	17.629	12.834	0.728
2	323	3.395	329.851	240.132	207.535	151.085	0.728
3	123	3.395	123.713	90.063	116.379	84.724	0.728
4	38	3.395	37.976	27.647	97.221	70.777	0.728
5	−40	1	−40.304	−29.341	2.253	1.640	0.728
6	28	1	28.349	20.638	0.338	0.246	0.728
I	100	1	100.707	98.592	13.874	13.583	0.979
II	250	1	252.977	247.664	72.900	71.369	0.979
III	60	1	60.347	33.312	4.764	2.630	0.552
IV	−30	1	−30.149	−16.642	0.756	0.417	0.552
PA3-CCTT-R							
1	108	1	108.808	53.076	16.108	7.857	0.488
2	267	2.639	271.644	132.507	157.572	76.863	0.488
3	117	2.639	117.892	57.508	94.839	46.262	0.488
4	267	6.516	271.644	132.507	228.455	111.440	0.488
5	117	6.516	117.892	57.508	165.722	80.839	0.488
6	37	6.516	37.048	18.072	148.228	72.305	0.488
7	29	5.834	28.813	14.055	138.675	67.645	0.488
8	57	5.834	57.103	27.855	142.486	69.504	0.488
9	−54	1	−54.452	−26.562	5.209	2.541	0.488
10	28	1	27.964	13.641	0.302	0.147	0.488

(*Continued*)

Table A2. Continued.

No.	T (°C)	p (bar_g)	h (kJ/kg)	$\dot{H}$(kW)	ex (kJ/kg)	$\dot{E}x$ (kW)	$\dot{m}$ (kg/s)
I″	100	1	100.707	49.279	13.874	6.789	0.489
II″	250	1	253.977	124.279	72.900	35.673	0.489
I′	100	1	100.707	49.279	13.874	6.789	0.489
II′	250	1	253.977	124.279	72.900	35.673	0.489
III	60	1	60.347	36.011	4.764	2.843	0.597
V	37	1	37.222	22.212	1.284	0.766	0.597
IV	−30	1	−30.149	−17.991	0.756	0.451	0.597
I	100	1	100.707	98.559	13.874	13.578	0.979
II	250	1	253.977	248.559	72.900	71.345	0.979

Table A3. Logarithmic mean temperature difference of the heat exchanger.

Component	ΔT_m (K)
PA0-R	
HTHX	43.29
LTHX	18.91
IHX	9.51
PA3-CCTT-R	
HTHX1	17.01
HTHX2	17.01
LTHX1	5.39
LTHX2	15.50
IHX	9.00